University of Alberta Library
0 1620 2669895 9

Ex Libris
Universitatis
Albertaensis

UNIVERSITY OF ALBERTA

*RELEASE FORM*

NAME OF AUTHOR: Guanghong Zhang

TITLE OF THESIS: A Computational Approach to Joint Torque Sensing of Manipulators

DEGREE: Masters of Science

YEAR THIS DEGREE GRANTED: 1992

Permission is hereby granted to UNIVERSITY OF ALBERTA LIBRARY to reproduce single copies of this thesis and to lend or sell such copies for private, scholarly or scientific research purposes only.

The author reserves other publication rights, and neither the thesis not extensive extracts from it may be printed or otherwise reproduced without the author's permission.

University of Alberta

# A Computational Approach to Joint Torque Sensing of Manipulators

by

Guanghong Zhang

©

A thesis
submitted to the Faculty of Graduate Studies and Research
in partial fulfillment of the requirements for the degree
of Masters of Science

Department of Computing Science

Edmonton, Alberta
Spring 1992

UNIVERSITY OF ALBERTA

FACULTY OF GRADUATE STUDIES AND RESEARCH

The undersigned certify that they have read, and recommend to the Faculty of Graduate Studies and Research, for acceptance, a thesis entitled **A Computational Approach to Joint Torque Sensing of Manipulators** submitted by **Guanghong Zhang** in partial fulfillment of the requirements for the degree of Masters of Science.

To my wife **Feng Luo**
and
my brother **Guangjun Zhang**

# Abstract

Joint torque sensing represents a critical step towards a number of promising force control methods. In this thesis, we proposed and implemented a computational approach to joint torque sensing based on sensor data fusion for an industrial robot. Joint torque obtained in this way may be used in many ways.

Sensor data fusion is the process of combining different sources of information to infer a consensus view on the environment. The proposed method uses two sources of indirect and noisy inputs, motor currents and wrist mounted torque/force sensor, to estimate optimally the actual torque exerted by robot joints. In order to demonstrate the feasibility of the proposed method, we specially design a single-joint robot. Parameter identification of the single-joint robot is formulated and experimentally carried out. Error associated with each sensor is analyzed in detail and the statistical *a priori* knowledge is derived. An evaluation procedure for sensor data fusion based on the *a priori* knowledge is developed. Robustness of the proposed technique to unmodeled disturbances is discussed and demonstrated via experiments. Possible extension of work done in our experimental system to a six DOF robot in general is summarized.

# Acknowledgments

I would like to thank, first of all, my supervisor, Dr. Hong Zhang, for his patience, detailed guidance and support throughout this research. I'd also like to thank my examining committee members, Dr. A. Basu, Dr. P. Wojcik and Dr. V. G. Gourishankar, for their careful review of the thesis and helpful suggestions.

Many people deserve special thanks. Mr. S. Sutphen spent much effort to build the experimental system. Mrs A. Altmann, a wonderful lady, helped me correct my poor English grammar and make this version of thesis more readable. Also, a special thanks goes to people working in the Robotics/Vision Lab for helpful discussions.

Finally, I am in deep debt to my wife. This thesis would certainly be in the air without her devoted love and care. My wholehearted thanks for *everything* she has done to me.

# Contents


**1 Introduction** **1**

1.1 Introduction . . . . . 1

1.2 Method We Propose . . . . . 3

1.3 Previous Work On Joint Torque Sensing . . . . . 3

1.4 Contribution . . . . . 5

1.5 Thesis Organization . . . . . 6

**2 Experimental System Description and Modeling** **7**

2.1 Overview of System Hardware . . . . . 7

2.2 Design of Single-Joint Robot System . . . . . 9

2.2.1 Selection of Strain Gauges and Practical Strain Gauge Measurement Concerns . . . . . 9

2.2.2 Link . . . . . 10

2.2.3 Extra Metal . . . . . 13

2.3 Parameter Identification in The Experimental System . . . . . 15

2.3.1 Least Square Fitting Technique for Parameter Identification . 16

2.3.2 Experiments On Parameter Identification . . . . . 17

2.4 Summary . . . . . 31

**3 Sensor Data Fusion** **33**

3.1 The Maximum-Likelihood Method . . . . . 34

3.2 An Overview of Sensor Data Fusion . . . . . 36

3.3 Summary . . . . . 38

**4 Joint Torque Sensing Based On Sensor Data Fusion** **39**

4.1 Actual Joint Torque . . . . . 40

4.2 Motor Current Derived Joint Torque . . . . . 40

4.3 Strain Gauge Derived Joint Torque . . . . . 45

4.4 Joint Torque Sensing Based on Sensor Data Fusion . . . . . 49

4.4.1 Fusion Algorithm . . . . . 49

4.4.2 Fusion Evaluation . . . . . 50

4.4.3 Fusion Heuristics . . . . . 53

4.5 Summary . . . . . 54

**5 Robustness of the Proposed Method to Unmodeled Disturbances** **56**

5.1 Case I: Motor Current is Disturbed by D1 . . . . . 58

5.2 Case II: Strain Gauge is Disturbed by D2 . . . . . 61

5.3 Case III: Both Sensors are Under Disturbances . . . . . 63

5.4 Summary . . . . . 66

**6 Conclusions** **68**

6.1 Conclusions . . . . . 68

6.2 Future Work . . . . . 69

# List of Figures


1 A Schematic Model of Single Joint Robot with Sensors . . . . . 8

2 Strain Gauge Measurement Principle . . . . . 10

3 Link Calculation . . . . . 12

4 Inertia Calculation . . . . . 12

5 Extra Metal . . . . . 14

6 Intersection of the Link . . . . . 15

7 Total Model of Experiment System with Parameters . . . . . 16

8 Motor Current Profile in One Revolution(Clockwise) . . . . . 18

9 Motor Current Profile in One Revolution(Counterclockwise) . . . . . 19

10 Repeatability Plot of Torque Ripples(Clockwise) . . . . . 20

11 Repeatability Plot of Torque Ripples(Counterclockwise) . . . . . 20

12 Velocity Starting Process(Clockwise) Under Different Voltages . . . . 23

13 Current Starting Process(Clockwise) Under Different Voltages . . . . 24

14 Velocity Starting Process(Counterclockwise) Under Different Voltages 24

15 Current Starting Process(Counterclockwise) Under Different Voltages 25

16 Least Square Solution of Motor Inertia(Clockwise) . . . . . 26

17 Least Square Solution of Motor Inertia(Counterclockwise) . . . . . 27

18 Linear Model of The Torque Constant . . . . . 30

19 Least Square Solution to End-Point Force Sensitivity . . . . . 32

20 Current Profile in Static Case, Desired Value is 700 . . . . . 42

21 Current Profile in Dynamic Case, Desired Value is 700 . . . . . 43

22 Variance Plot of Motor Current . . . . . 44

23 Readings Out of the Wheatstone Bridge . . . . . 46

24 Low-pass Filtered Output . . . . . 46

25 Variance Plot of Strain Gauge Derived Joint Torque . . . . . 48

26 Error Plot of 1st Set Data When $I$ is Under D1 . . . . . 59

27 Error Plot of 2nd Set Data When $I$ is Under D1 . . . . . 60

28 Error Plot of 1st Set Data When $V_{out}$ is Under D2 . . . . . 62

29 Error Plot of 2nd Set Data When $V_{out}$ is Under D2 . . . . . 63

30 Error Plot When Both Sensors are Under D3&D4 . . . . . 64

31 Error Plot When Both Sensors are Under D3&D4 . . . . . 65

# List of Tables


2.1 Friction in the Clockwise Direction . . . . . 21

2.2 Friction in the Counterclockwise Direction . . . . . 21

2.3 Inertia Identification in the Clockwise Direction . . . . . 24

2.4 Inertia Identification in the Counterclockwise Direction . . . . . 25

2.5 Resistor Identification in the Clockwise Direction . . . . . 27

2.6 Resistor Identification in the Counterclockwise Direction . . . . . 27

2.7 $K_{emf}$ Identification in the Clockwise Direction . . . . . 28

2.8 $K_{emf}$ Identification in the Counterclockwise Direction . . . . . 28

2.9 Experimental Data on Identifying Torque Constant . . . . . 29

2.10 Readings Out of The Wheatstone Bridge . . . . . 31

4.11 Motor Current Data Used for Deriving Statistics . . . . . 44

4.12 Strain Gauge Readings for Deriving Statistics . . . . . 47

4.13 Converted Value Based on Table 4.12 . . . . . 48

4.14 Fusion Weights for Both Sensors . . . . . 50

4.15 Two Sets of Data for Evaluation . . . . . 52

4.16 Evaluation of the First Set of Data . . . . . 52

4.17 Evaluation of the Second Set of Data . . . . . 53

5.18 A Collection of Normal Distributed Disturbances . . . . . 58
5.19 Evaluation of the First Set of Data Under D1 Disturbance . . . . . 59
5.20 Evaluation of the Second Set of Data Under D1 Disturbance . . . . . 60
5.21 Evaluation of the First Set of Data Under D2 Disturbance . . . . . 61
5.22 Evaluation of the Second Set of Data Under D2 Disturbance . . . . . 62
5.23 Evaluation of the First Set of Data Under D3&D4 Disturbances . . . 64
5.24 Evaluation of the Second Set of Data Under D3&D4 Disturbances . . 65
5.25 Summary of $\overline{e^2}$ for All Cases . . . . . 66
5.26 Summary of $\sigma^2$ for All Cases . . . . . 66

# Chapter 1

# Introduction

## 1.1 Introduction

Current industrial robots are almost unexceptionally position controlled devices. Many modern applications require accurate control of contact forces. For example, if a robot is to clean glass with a piece of sponge, the contact force between the robot's hand and the surface of the glass has to be controlled in order not to break the glass while maintaining the contact. Many methods have been proposed in literature[40, 44, 46, 30, 29]. Among them, joint torque control method is very promising and has been the focus of much attention[49, 33, 7, 38, 25, 32, 17, 26, 36, 27, 20]. Experiment results conducted by many researchers demonstrated that by accurate control of joint torque, the system could have wide bandwidth[49], and great reduction of nonlinear friction[33, 38]. In addition, torque based force control schemes are not hampered by environment stiffness and can therefore be used for robust hard-on-hard contact[17]. When applied in fine motion control, joint torque control can

also avoid "dynamic compensation" [25, 32] which is very difficult to carry out in real time. Also, disturbance torques caused by gear reducers and actuators can be compensated by joint torque feedback, and thus accuracy of motion control can be greatly improved. However, the issue of how to obtain joint torque remains a difficult one. Three distinct approaches to sensing joint torque have been attempted so far:

1. joint torque derived from wrist-mounted force sensor[40];
2. motor current calibrated against the motor shaft output torque[7]; and
3. redesign of the motor shaft mechanism to allow some sort of torque sensor to be mounted [38, 33, 26, 49, 17].

The first method results in "non-collocation" of sensor and actuator and is difficult to stablize[19, 18], while the second method is most useful in direct drive arms where uncertainty in friction is minimized because of the absence of reducer. The third method is very effective in reducing the nonlinear friction, and has been experimentally implemented on a number of industrial robots[33, 38]. Results obtained from these experiments show that the nonlinear friction can be reduced up to 97%. The disadvantage of this method is that the shaft mechanism to which the joint torque sensor is attached has to be redesigned so that room can be found for the sensor. This introduces many undesired problems. First, the stiffness of the shaft is decreased, which is not a good practice considering system bandwidth requirements. The effect might be magnified by the fact that there has to be a compromise between the stiffness of the shaft and the sensitivity of the sensor. Secondly, as different joints may employ different reducers, the output of the sensor may contain some undesired components due to the structure of some particular reducers[26]. This requires extra techniques of compensation which appear quite elusive[26]. Thirdly, physical limitation in some robot does not allow mounting of any sensors in the joint mechanism.

## 1.2 Method We Propose

We propose a computational technique to obtain joint torque indirectly in cases where direct mounting of torque sensors is impossible or undesirable. In addition, obtaining the joint torque indirectly may provide an effective way to monitor the condition of joint torque sensors. In case of a sensor failure, any algorithm based on a single sensor will fail to work properly. By detecting torque sensor failure, the proposed approach may become the basis for robust robot control systems[28] and logic sensor[50] for intelligent robot systems.

On the other hand, recent interests in studying sensor fusion techniques and applications by many researchers[10, 23, 43, 16, 42, 8, 34, 24, 22, 1, 28, 3, 50, 2] lead us to believe that by combining information from different sensors it is possible to extract more accurate information than any single sensor can provide. Our proposed method uses two sources of indirect and noisy inputs, motor currents and wrist mounted torque/force sensor, to optimally estimate the actual torque exerted by the joint. For fusion technique, we employ the Maximum-Likelihood(ML) method to effectively combine two sources of information based on the *a priori* knowledge obtained from a large number of experiments. To emphasize the difference between our method and other joint torque sensing techniques which are hardware dependent, the proposed method is termed as "computational approach".

## 1.3 Previous Work On Joint Torque Sensing

As early as 1980, Wu and Paul[49] did the pioneer work, "manipulator compliance based on joint torque control", on a single joint manipulator. The sensor system

consisted of four semiconductor strain gauges mounted on the circular aluminum joint shaft to form a zero balance Wheatstone Bridge. A high gain, wide bandwidth torque servo using the sensor system was implemented, and experimental results showed that more than 95 percent of effective friction was reduced for motion control. A number of other issues like collision with environment and the effect of steady state error while changing velocity gain and torque gain were also studied. Encouraged obviously by results of Wu and Paul, Luh *et al.*[33] moved the experiment from single joint manipulator to industrial robots. Two joints of the Stanford manipulator were redesigned and fabricated to include torque sensing capability by means of strain gauges. The resulting control systems reduced the effective friction from 1072 oz·in to 33.5 oz·in. Stability analysis of the total system was also carried out, and a phase-lead compensation network was inserted. Asada *et al.*[7] for the first time studied joint torque sensing techniques for a direct-drive arm and the performance of the resulting system was analyzed. Two schemes of joint torque sensing, an indirect method via current measurement and a direct method using strain gauges, were proposed. They developed a design principle to achieve high sensitivity torque measurement without sacrificing the high mechanical stiffness, and later verified it through experiments. Khatib *et al.*[38] carried out torque control experiment on PUMA 500. They designed and implemented a joint torque servomechanism. Experimental results obtained from pure torque control and joint motion tracking demonstrated a significant reduction of the effective friction(97%) and a substantial improvement in fine motion control. Hashimoto[25] presented a new joint torque sensing technique using the elasticity of the harmonic drive. A new control scheme based on the joint torque feedback was proposed by him for robot motion control. The new scheme had two distinctive features: the real time dynamic compensation is not required, and it is robust to disturbances such as variable load. Further, he and others[26] presented in detail joint torque sensing techniques for robots with harmonic drives.

Combination of motor current and the end-point force sensor for force control has been experimentally studied by An and Hollerbach[5] on a single-link MIT DDArm. They aimed to verify through experiment that the system has a higher bandwidth and better steady state force tracking error than the use of any single one of these sensors. We noted that their conclusion was drawn from experiments on DDArm where joint friction is insignificant. Therefore, it may not be applicable to systems where nonlinear friction introduced mainly by reducer is significant, such as an industrial robot. Most importantly, no efforts were made in their work to study sensor data fusion.

## 1.4 Contribution

We proposed a computational approach to joint torque sensing based on sensor data fusion for an industrial robot. The main contribution of this work is experimental. A single-joint model of a typical industrial robot is designed to demonstrate the feasibility of the proposed method. The proposed joint torque sensing method is studied thoroughly in the static case and extension of the proposed method to the dynamic case is discussed. Parameter identification of the model is formulated and experimentally carried out. Most of the identification procedures are directly applicable to a six DOF robot in general. We also provide a framework to carry out sensor data fusion and evaluate fusion results. Robustness of the proposed joint torque sensing to unmodeled disturbances is discussed and demonstrated via experiments on the single-joint model.

## 1.5 Thesis Organization

Chapter 1 introduces the problem and the work previously done. Also, the computational approach we proposed is stated.

Chapter 2 is focused on the experiment system design and its mathematical model establishment.

Chapter 3 gives an overview of sensor data fusion and elaborates on the Maximum-Likelihood(ML) method.

Chapter 4 presents in detail the proposed joint torque sensing method. Error associated with each sensor is analyzed and statistics of each sensor are derived. Also, an evaluation procedure for sensor data fusion is developed.

Chapter 5 discusses robustness of the proposed method to unmodeled disturbances via experimental results.

Chapter 6 concludes this thesis and possible future works are overviewed.

# Chapter 2

# Experimental System Description and Modeling

In order to demonstrate the feasibility of the proposed method to sense joint torque, a single-joint robot is designed. This chapter is organized as follows. First, an overview of the system hardware is conducted. Then, selected design details are presented. Further, parameter identification of the single-joint robot is formulated and experimentally carried out. Finally, a summary concludes the work, and the extension of parameter identification to a six DOF robot is briefly stated.

## 2.1 Overview of System Hardware

In this section we briefly describe the experiment hardware of our single-joint robot. Basically, the whole system consists of two subsystems, namely, Motor-Reducer-Shaft(MRS) subsystem and Link-Strain Gauge(LSG) subsystem. Figure 1 shows

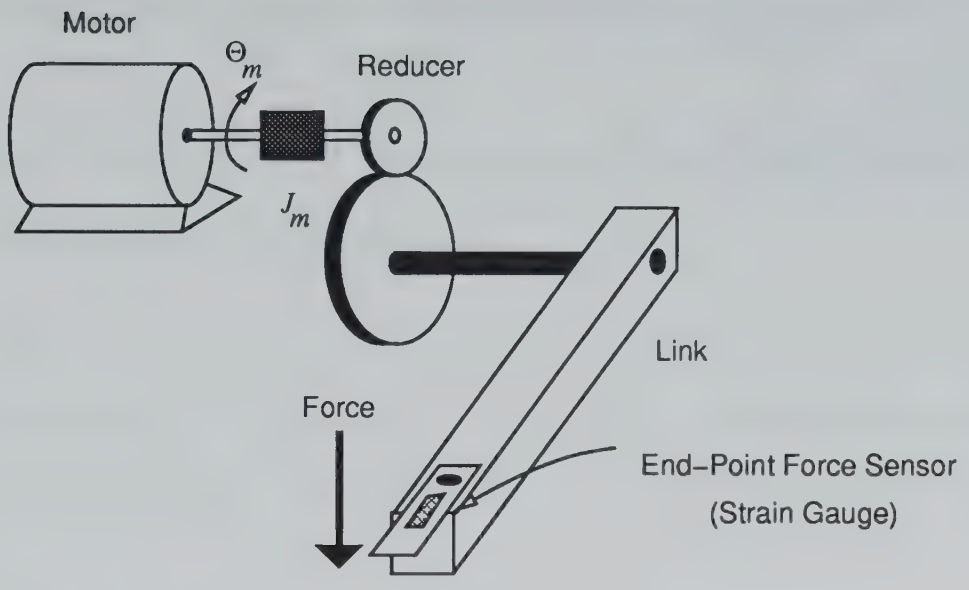


Figure 1: A Schematic Model of Single Joint Robot with Sensors

the model. A permanent magnetic motor is selected which has torque capacity of 24 oz·in. The motor is then connected to a reducer of gear ratio 60, which is close to that of a real robot. The output shaft of the reducer is coupled via a connecting shaft to the link which simulates the arm of a real robot. The connecting shaft is designed in such a way that as little as possible joint flexibility is allowed. The link is also carefully designed according to capacity of the motor. Since the link is too wide to bend, strain gauge and its electronics mounted directly on the tip-of-link will not result in any useful readings. To overcome the difficulty, an extra piece of metal is designed and put near the tip-of-link. Strain gauge is then put on top of the extra metal. Detailed design follows in next section.

## 2.2 Design of Single-Joint Robot System

### 2.2.1 Selection of Strain Gauges and Practical Strain Gauge Measurement Concerns

The strain gauge is a transducer used for the measurement of dimensional variations in a mechanical system. It is based on the principle that electric resistance within a conductor varies with respect to a change in its physical dimensions, its length for example.

There are many important characteristics for a strain gauge. The most important is the sensitivity or generally known as *gauge factor* which is defined as the ratio between the unit change in electric resistance and the unit change in physical length, shown mathematically as[37]

$$G_f = \frac{\Delta R/R}{\Delta L/L} \tag{2.1}$$

Together with other important characteristics such as nominal resistance, maximum elongation, fatigue properties, temperature characteristic and physical dimensions, $G_f$ can be easily obtained from the manufacturer's booklet. Selection of strain gauge in our experiment is first subject to physical requirement: the space that the strain gauge is allowed to take up. $G_f$ and other important characteristics as noted are chosen accordingly. Shown in Figure 2 is a Wheatstone bridge to measure strain which consists of three reliable resistors and a strain gauge in a quarter bridge configuration. There are other possible configurations such as half bridge(two strain gauges) and full bridge(four strain gauges) in practice, both of which are good at temperature compensation which may be crucial in some applications. The reasons for choosing the quarter bridge configuration are, first of all, the environment temperature is not a major factor in our experiments, secondly, higher sensitivity of the strain gauge

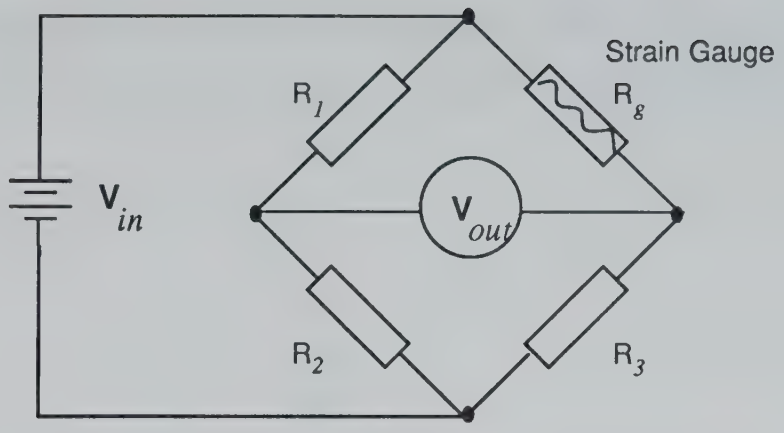


Figure 2: Strain Gauge Measurement Principle

is desirable, and thirdly the space for mounting such strain gauge is comparatively small.

The calculation of strain from Figure 2 goes as follows. It can be easily derived from the Wheatstone bridge that the following relation holds

$$V_{out} = \left[\frac{R_3}{R_3 + R_g} - \frac{R_2}{R_1 + R_2}\right] V_{in} \tag{2.2}$$

Defining,

$$V_r = \left[(\frac{V_{out}}{V_{in}})_{strained} - (\frac{V_{out}}{V_{in}})_{unstrained}\right] \tag{2.3}$$

we can obtain by some mathematical manipulation that

$$\frac{\Delta R_g}{R_g} = \frac{-4V_r}{1 + 2V_r} \tag{2.4}$$

According to definition ( 2.1), the strain becomes

$$\varepsilon = \frac{-4V_r}{G_f(1 + 2V_r)} \tag{2.5}$$

### 2.2.2 Link

Given the system characteristics, such as motor capacity, gear ratio, friction etc., we want to determine the dimension of the link so that the designed link will not be

too big or too small. This includes calculation of length, width, and thickness of the link. We make use of Lagrange's result(as applied to robotics)[9] which can be briefly written as

$$K = K_1 + K_2 + \cdots + K_n = \sum_{i=1}^{n} K_i \tag{2.6}$$

$$\frac{d}{dt}\left[\frac{\partial K}{\partial \dot{\theta}_i}\right] - \frac{\partial K}{\partial \theta_i} = M_i, i = 1, 2, \cdots, n \tag{2.7}$$

where each $K_i$ is known as kinematic energy of frame $i$, $\theta_i$ is the coordinate of frame $i$ on which $K_i$ is defined, $\dot{\theta}_i$ is its corresponding velocity and $M_i$, the applied force/torque. Assume that $v_i$ represents the velocity of the center of mass relative to the base, $\omega_i$ represents the angular velocity of the body relative to the base; $I_i$ represents the inertia matrix of the body relative to frame $i$ when frame $i$ is translated to the center of mass of the body and finally, $T$ represents the transpose of a matrix, the kinematic energy $K_i$ is defined as:

$$K_i = \frac{1}{2} m_i v_i^T v_i + \frac{1}{2} \omega_i^T I_i \omega_i \tag{2.8}$$

Now we apply the above result to design the link. Suppose $l, w, t$ represent the length, width and thickness respectively, and the material of the link is uniformly distributed, i.e. its density $\rho$ is constant, we have the following(see Figure 3)

$$K = \frac{1}{2} m v^2 + \frac{1}{2} I \dot{\theta}^2 = \frac{1}{8} m l^2 \dot{\theta}^2 + \frac{1}{2} I \dot{\theta}^2 \tag{2.9}$$

where $m = \rho \cdot l \cdot w \cdot t$ and $I$ is calculated as follows(Figure 4)

$$I = \int_0^t \int_{-l/2}^{l/2} \int_{-w/2}^{w/2} \rho \cdot (x^2 + y^2) dx dy dz = \frac{1}{12} m (w^2 + l^2) \tag{2.10}$$

Therefore,

$$K = \frac{1}{24} m (w^2 + 4l^2) \dot{\theta}^2 \tag{2.11}$$

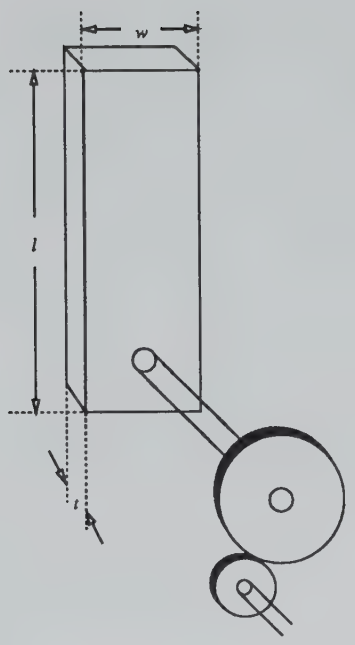


Figure 3: Link Calculation

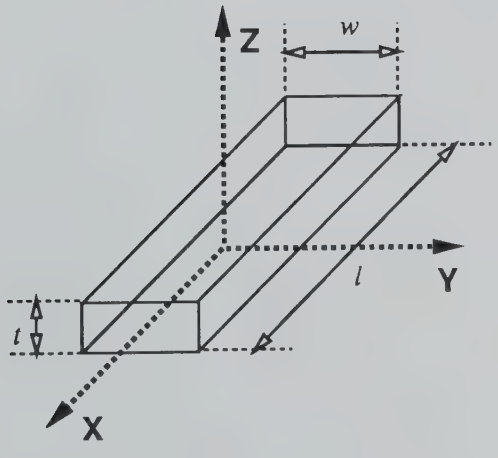


Figure 4: Inertia Calculation

Apply equation( 2.7), the following is obtained:

$$\frac{1}{12}m(w^2 + 4l^2)\ddot{\theta} = M \tag{2.12}$$

Assume the gear ratio is $n(\geq 1)$, and friction of the system is $f$,then

$$M = nM_{motor} - f - mg \cdot \frac{l}{2}cos\theta \tag{2.13}$$

Examine equation( 2.9)( 2.12) and ( 2.13), it is easy to conclude that given $\rho$, $M_{motor}$, $f$, $\ddot{\theta}$, we have an equation which combine $w, t, l$ together. Therefore, assuming any two of these three parameters, the third one is determined. Specifically, assuming $w, t$ are known, and $cos\theta = 1$, we have

$$\frac{1}{3}\rho wt\ddot{\theta}l^3 + \frac{1}{2}\rho wtgl^2 + \frac{1}{12}\rho w^3 t\ddot{\theta}l = nM_{motor} - f \tag{2.14}$$

By solving the above equation, we get the desired dimension of the link.

### 2.2.3 Extra Metal

Being the end-point force sensor, the strain gauge has to reflect how much force is applied upon the tip of the link. Obviously, if strain gauge and its associated electronics are mounted directly on the tip, we will not be able to get any useful readings simply because the link is too wide to bend. A special piece of thin metal(we call it extra metal) has to be designed. The guideline for the design is high sensitivity while not destroying the sensor.

Analytical expressions relating bending moment to stress at a section of a beam is well established[39] and is shown as

$$\sigma_{max} = \frac{Mc}{I} \tag{2.15}$$

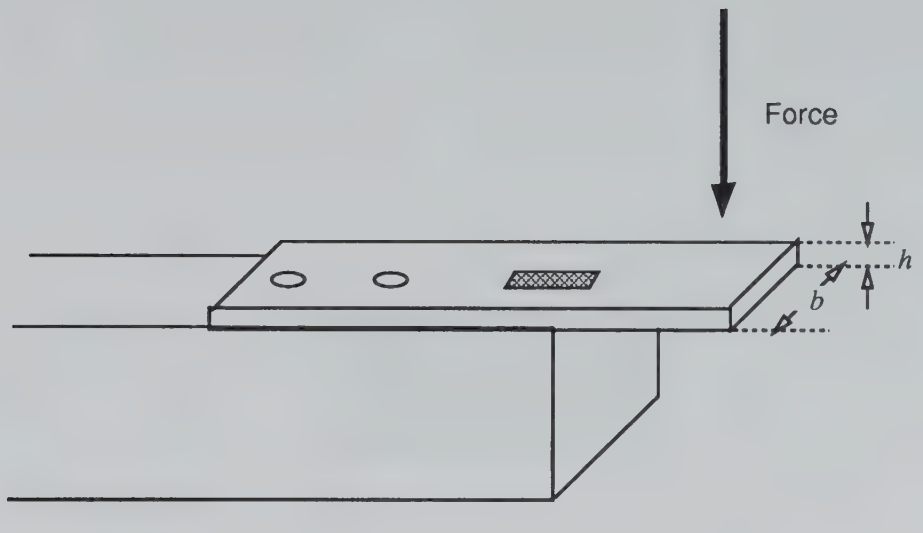


Figure 5: Extra Metal

where $M$ is the bending moment, $c$ is the distance from the centroidal axis to the surface where maximum stress is resulted, and $I$ is the moment of inertia about the centroidal axis. For any particular material, $I$ is a constant. The strain can therefore be written as

$$\varepsilon_{max} = \frac{\sigma_{max}}{E} \tag{2.16}$$

where $E$ is known as Young's modulus. Since the strain is much smaller compared to the size of the metal, we assume the uniform distribution of stress upon the strain gauge(Figure 5). From the definition of strain, which is

$$\varepsilon = \frac{\Delta}{L} \tag{2.17}$$

where $\Delta$ is the elongation of the sensor and $L$ is the length of the sensor. From Figure 6, $c = h/2$, and $I = bh^3/12$. So,

$$\Delta = \frac{L}{E} \cdot \frac{6M}{bh^2} \tag{2.18}$$

As we know the maximum elongation of the strain gauge and the maximum force acting upon the tip, assuming any value for $b$ will uniquely determine the value of $h$.

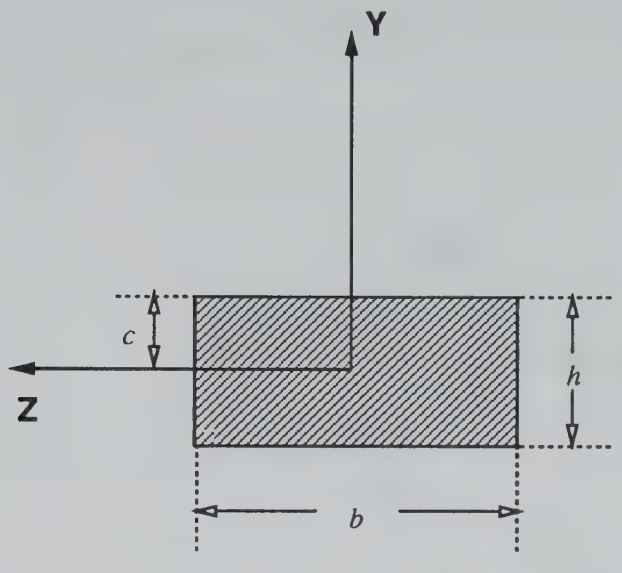


Figure 6: Intersection of the Link

## 2.3 Parameter Identification in The Experimental System

It is well-known that model-based control can greatly improve system performance[4]. However, it is difficult to obtain an accurate model of a system. There have been interests in studying algorithms that identify system parameters[45, 31, 48, 14, 41]. The parameter identification problem is the estimation of parameters via external measurements.

The total model of our experiment system together with parameters to be identified is shown in Figure 7. We will first briefly state the least square fitting technique for parameter identification and then experimentally carry on the identification.

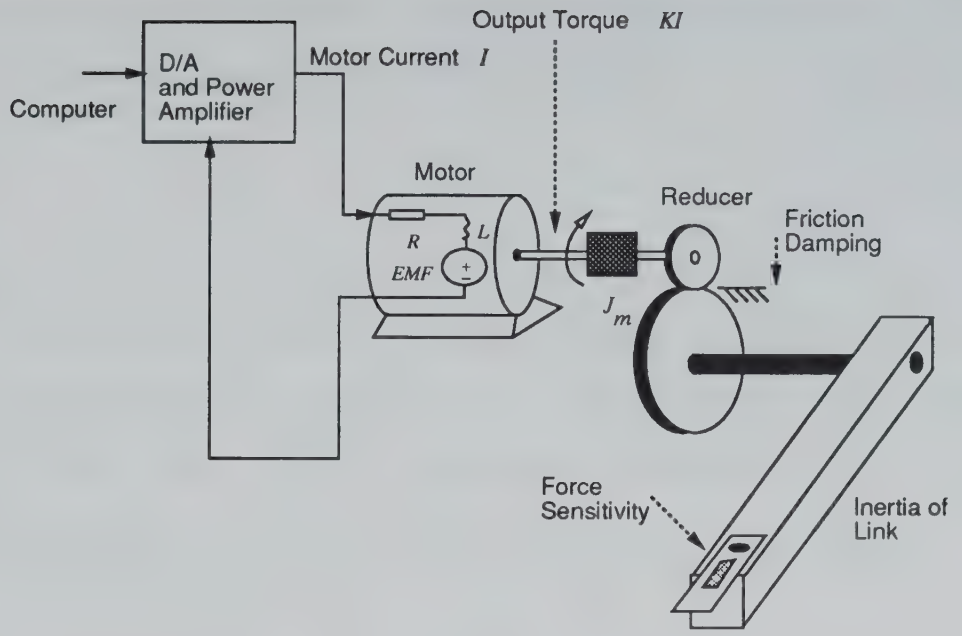


Figure 7: Total Model of Experiment System with Parameters

### 2.3.1 Least Square Fitting Technique for Parameter Identification

Suppose the following relation holds:

$$\mathbf{Z} = \mathbf{H}\alpha + \vartheta \tag{2.19}$$

where $\mathbf{Z}$ is an $m \times 1$ measurement vector, $\alpha$ is an $n \times 1$ vector of parameters to be estimated, $\mathbf{H}$ is a $m \times n$ matrix which relates the parameters and output measurements, and $\vartheta$ is a $m \times 1$ vector of measurement noise. The least square solution to the above equation is well known[21]:

$$\hat{\alpha} = \left[\mathbf{H}^T\mathbf{H}\right]^{-1}\mathbf{H}^T\mathbf{Z} \tag{2.20}$$

where $\hat{\alpha}$ is the Least Square estimate of $\alpha$, and the superscript $T$ represents matrix transpose.

Given $\mathbf{Z}$ and $\mathbf{H}$, $\hat{\alpha}$ can be thus calculated. However, given a particular identification

problem, exact format of $\mathbf{Z}$ and $\mathbf{H}$ is dependent on the definition of $\alpha$. For example, suppose we have a linear model of the following form

$$y = ax + b$$

where $y$ and $x$ are the measurement and input, and $a$ and $b$ are parameters to be identified. In other words, we try to identify the linear relationship between $y$ and $x$ which will be frequently encountered later on. Suppose further that we collect up to $n$ values for both $y$ and $x$. The least square fitting technique in this particular case becomes: Assuming $\alpha = \begin{bmatrix} a \\ b \end{bmatrix}$, $\mathbf{H}$ and $\mathbf{Z}$ will accordingly have the form

$$\mathbf{H} = \begin{bmatrix} x_1 & 1 \\ x_2 & 1 \\ \vdots & \\ x_n & 1 \end{bmatrix} \qquad \mathbf{Z} = \begin{bmatrix} y_1 \\ y_2 \\ \vdots \\ y_n \end{bmatrix}$$

Substitute $\mathbf{H}$ and $\mathbf{Z}$ into equation( 2.19) and the least square solution of $a$ and $b$ will be instantly obtained. In the remainder of this section, we will describe the formulation of each problem, definition of $\alpha$, experimental data on $\mathbf{Z}$ and $\mathbf{H}$, and finally solutions without detailed calculations.

## 2.3.2 Experiments On Parameter Identification

### 2.3.2.1 Torque Ripples

A DC motor with a permanent magnet is used in our experiment. The rotor is composed of a fixed number of windings that go through the magnetic field to produce the output torque. Because there are only a finite number of windings on the rotor, a

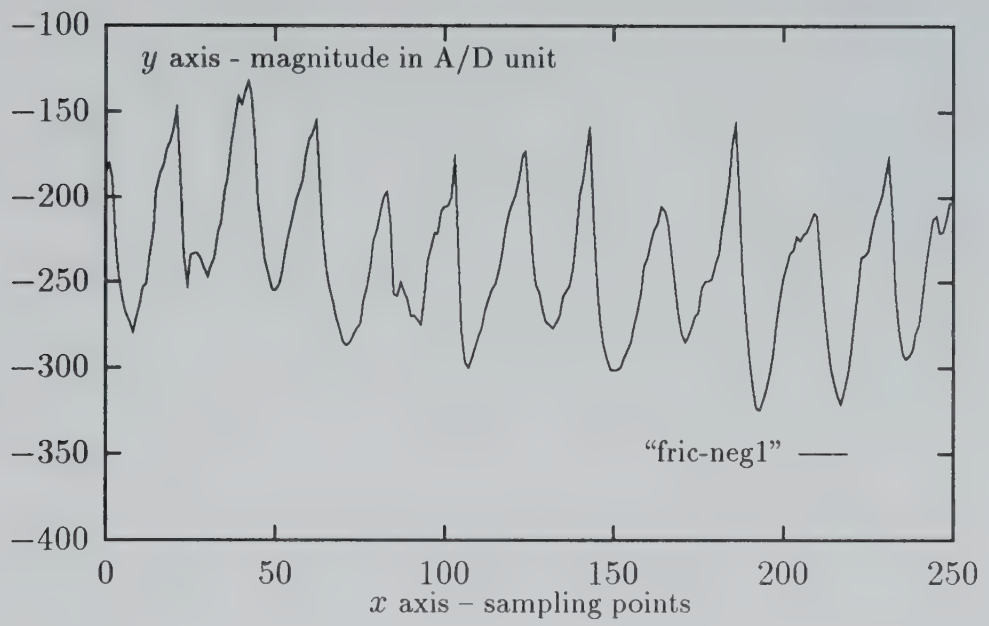


Figure 8: Motor Current Profile in One Revolution(Clockwise)

periodic magnetic field is generated. This results in a nonlinear relationship between rotor current and output torque and is called torque ripple. Depending on the actual structure of a particular DC motor, torque ripples might cause nonlinear torque and motor current relationship. To improve the performance, it is desirable to compensate the effect. As to our experiment system, the torque ripples consist of 12 periodic signals in each revolution of the motor shaft. This can be clearly seen from Figure 8 and Figure 9, the former is the recording of motor current in the clockwise direction while the latter is in the counterclock direction.

It is clear that torque ripples in our experiment system are not acceptable. The magnitude in the worst case is as large as that of static friction. Obviously, it is not easy to find an exact mathematical model for the torque ripples. One way to compensate for torque ripples is to use sine function to simulate current changes. Another way is to build a static table $\tau_r[index]$ which contains changes of torque ripples. At each sampling instance, the motor position is measured and converted

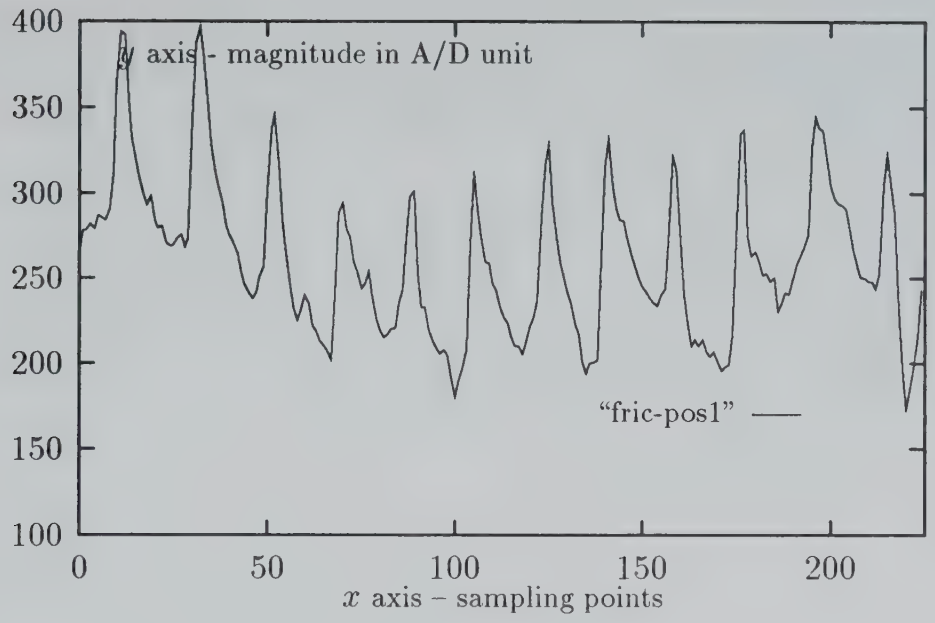


Figure 9: Motor Current Profile in One Revolution(Counterclockwise)

to the index that correctly looks up the position dependent torque value from the static table. This method requires the repeatability of the torque ripples. Figure 10 and Figure 11 show the comparison between two independent recordings in both directions. The curve in thin lines is the same as in Figure 8 and Figure 9, while the curve in thick lines is recordings for another revolution starting from the same initial position. There is not much discrepancy in the comparison. Therefore, the static table look-up technique is sufficiently accurate. To avoid the problem caused by the slight shift of initial position, the table can be constructed by averaging many samples from the same initial position.

#### 2.3.2.2 Friction

Friction models and compensation algorithms have been extensively studied in literature[13, 45, 6]. In spite of that, new models and new compensation algorithms

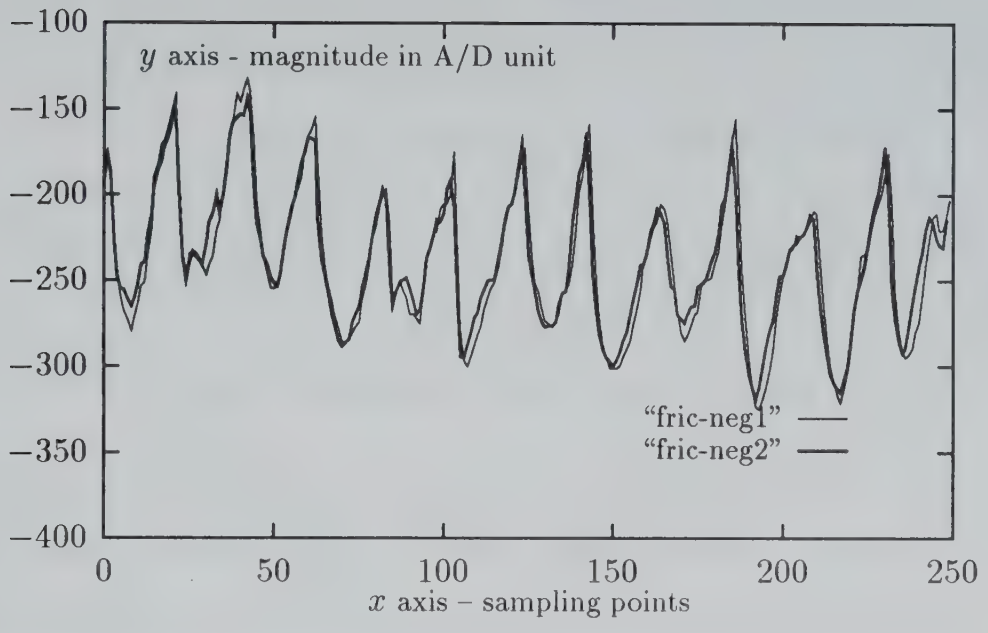


Figure 10: Repeatability Plot of Torque Ripples(Clockwise)

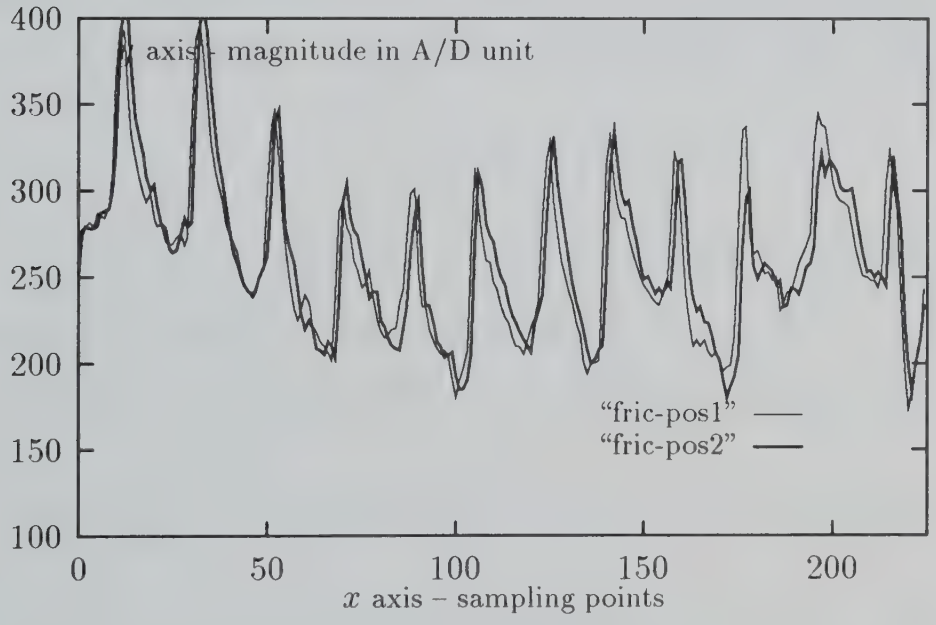


Figure 11: Repeatability Plot of Torque Ripples(Counterclockwise)

| Friction in Terms of Motor Current(in A/D unit) | 227 | 223 | 231 | 234 | 237 | 239 | 242 | 243 |
|---|---|---|---|---|---|---|---|---|
| Angular Velocity $\dot{\theta}$ | 5 | 6 | 8 | 9 | 11 | 13 | 14 | 16 |

Table 2.1: Friction in the Clockwise Direction

| Friction in Terms of Motor Current(in A/D unit) | 239 | 244 | 249 | 252 | 257 | 262 | 266 | 270 |
|---|---|---|---|---|---|---|---|---|
| Angular Velocity $\dot{\theta}$ | 5 | 6 | 8 | 10 | 11 | 13 | 15 | 16 |

Table 2.2: Friction in the Counterclockwise Direction

are still research topics[15]. It is generally agreed that the friction has two components, namely, Coulomb friction and viscous friction. The fact that the Coulomb friction is subject to uncertainty and the relation between friction and velocity is not linear makes friction compensation algorithms very complicated and not as satisfactory as expected. In fact, it is recently revealed that the viscous friction became negative at low velocities[6, 15]. Instead of studying complicated friction compensation algorithms, we adopt the Coulomb-plus-viscous friction model for simplicity, just as other researchers did[47, 45, 13]. The Coulomb-plus-viscous model has the form

$$F = f_s + f_v \cdot \dot{\theta} \tag{2.21}$$

where $\dot{\theta}$ is the velocity, and $f_s$ and $f_v$ are the Coulomb friction constant and viscous constant to be identified. Experimental data on friction $F$ and angular velocity $\dot{\theta}$ of both directions are recorded in Table 2.1 and Table 2.2 respectively.

Let us define $\alpha = \begin{bmatrix} f_v \\ f_s \end{bmatrix}$, and the least square solution to equation ( 2.21) based on data in Table 2.1 and Table 2.2 for both directions are: $\alpha_{cw} = \begin{bmatrix} 1.75 \\ 217 \end{bmatrix}$ and $\alpha_{ccw} =$

$\begin{bmatrix} 2.67 \\ 227 \end{bmatrix}$ where subscripts *cw* and *ccw* stand for the clockwise and counterclockwise direction respectively.

#### 2.3.2.3 Inertia $J_{link}$ and $J_{motor}$

The calculation of $J_{link}$ is relatively easy, and can be done in the same way as in equation( 2.10). The identification of $J_{motor}$ is difficult in a six DOF robot because of the rigid coupling of machine parts. The following method is believed to give a fairly accurate result in our system.

Experiments were carried out in MRS subsystem. The other half subsystem is totally disconnected. The following relation can be obtained by inspecting the subsystem:

$$K_I I - F = J_{motor} \cdot \ddot{\theta} \tag{2.22}$$

where $K_I$ is the torque constant, $\ddot{\theta}$ is the angular acceleration of the motor and $F$ is the friction in torque unit. This can be explained as the torque generated by the motor being partially used to overcome the friction and partially used to overcome the motor inertia. It is very important to realize that the starting process is crucial to the identification of motor inertia because $\ddot{\theta}$ is maximized during the starting process. Motor current also reaches its peak value. The signal-to-noise ratio in this case becomes very high and therefore the identified motor inertia is accurate. In our experiment system, $F$ is expressed in terms of motor current. Therefore, we have equation

$$I - F = \frac{J_{motor}}{K_I} \cdot \ddot{\theta} \tag{2.23}$$

Integrate both sides, assuming sampling period $\delta t$ is small:

$$\sum_{j=0}^{j=n} (I_j - f_s - f_v - \tau_r[j]) \cdot \delta t = \frac{J_{motor}}{K_I} \left( \dot{\theta}_{final} - \dot{\theta}_{initial} \right) \tag{2.24}$$

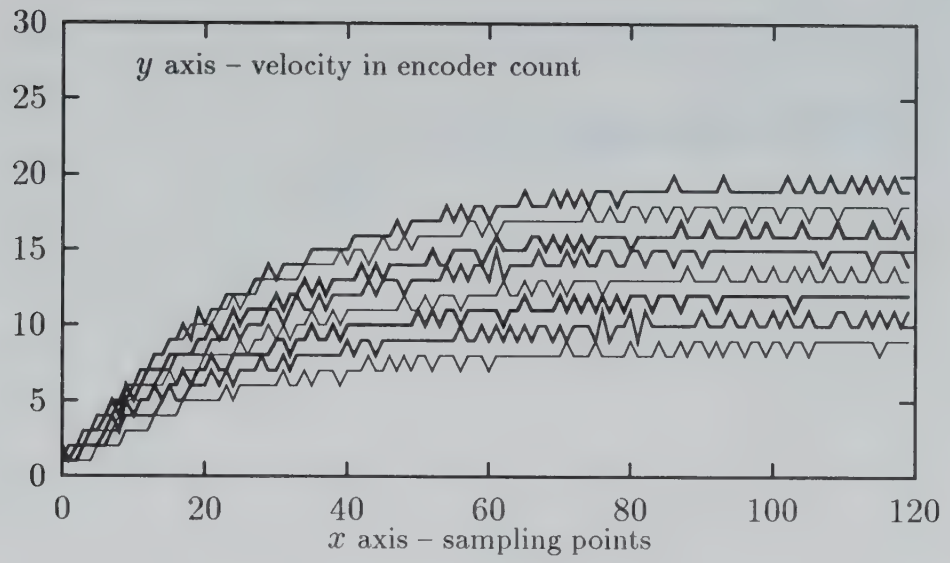


Figure 12: Velocity Starting Process(Clockwise) Under Different Voltages

Note that we substitute $F$ with the friction model stated before. We choose $\dot{\theta}_{initial} = 0$, so that

$$\sum_{j=0}^{j=n} (I_j - f_s - f_v - \tau_r[j]) \cdot \delta t = \frac{J_{motor}}{K_I} \cdot \dot{\theta}_{final} \tag{2.25}$$

which can be further written as

$$\sum_{j=0}^{j=n} (I_j - f_{static} - f_{viscous} - \tau_r[j]) = J'_{motor} \cdot \dot{\theta}_{final} \tag{2.26}$$

where $J'_{motor} = \frac{J_{motor}}{K_I \cdot \delta t}$. Figure 12 and Figure 13 show the starting processes of both velocity and motor current under different applied voltages, while Figure 14 and Figure 15 show the processes in the other direction. We choose $n$ to be 20 from these figures. Experiment data on the summation of the left-hand side of equation ( 2.26) and $\dot{\theta}_{final}$ are in Table 2.3 and Table 2.4 for both directions.

Assume $\alpha = J'_{motor}$, the least square solution to equation ( 2.26) for both directions are: $\alpha_{cw} = J'_{motor} = 1793.4167$ and $J_{motor} = J'_{motor} \cdot K_I \cdot \delta t = 1793.4167 \times 1.25 \times 10^{-3} \cdot K_I = 2.2418 K_I$; and $\alpha_{ccw} = J'_{motor} = 1611.1296$, and $J_{motor} = J'_{motor} \cdot K_I \cdot \delta t =$

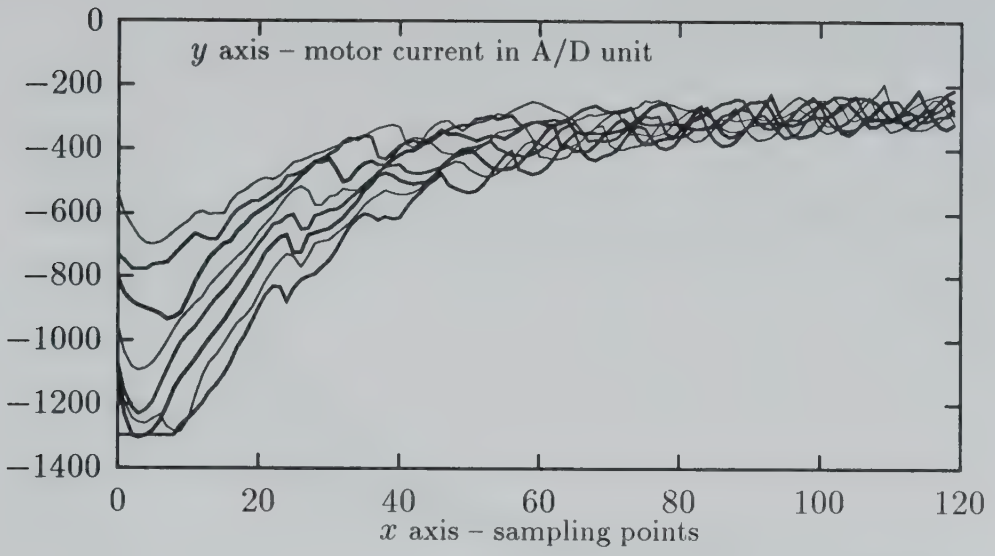


Figure 13: Current Starting Process(Clockwise) Under Different Voltages

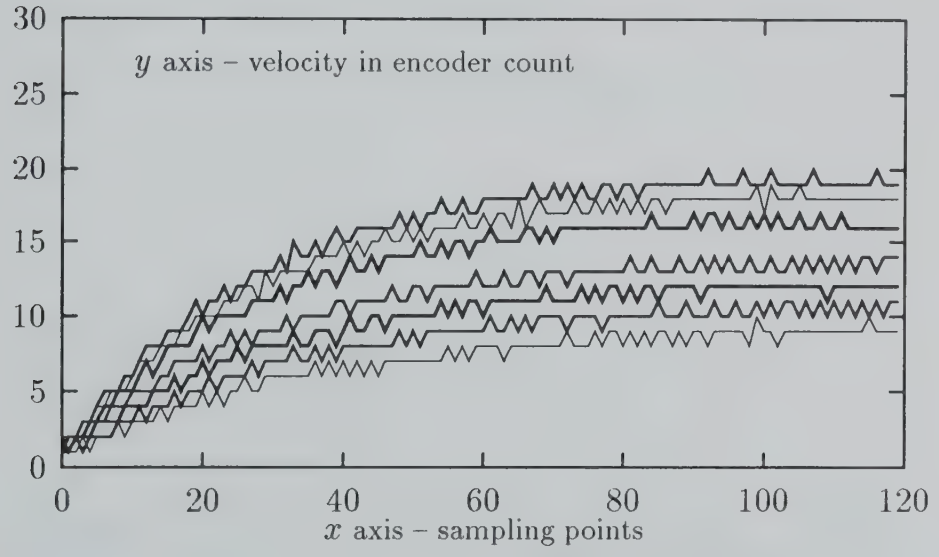


Figure 14: Velocity Starting Process(Counterclockwise) Under Different Voltages

| Summation in A/D Unit | 7985 | 9561 | 11743 | 13824 | 15506 | 17303 | 18314 | 19586 |
|---|---|---|---|---|---|---|---|---|
| $\dot{\theta}_{final}$ | 5 | 6 | 7 | 8 | 8 | 9 | 10 | 11 |

Table 2.3: Inertia Identification in the Clockwise Direction

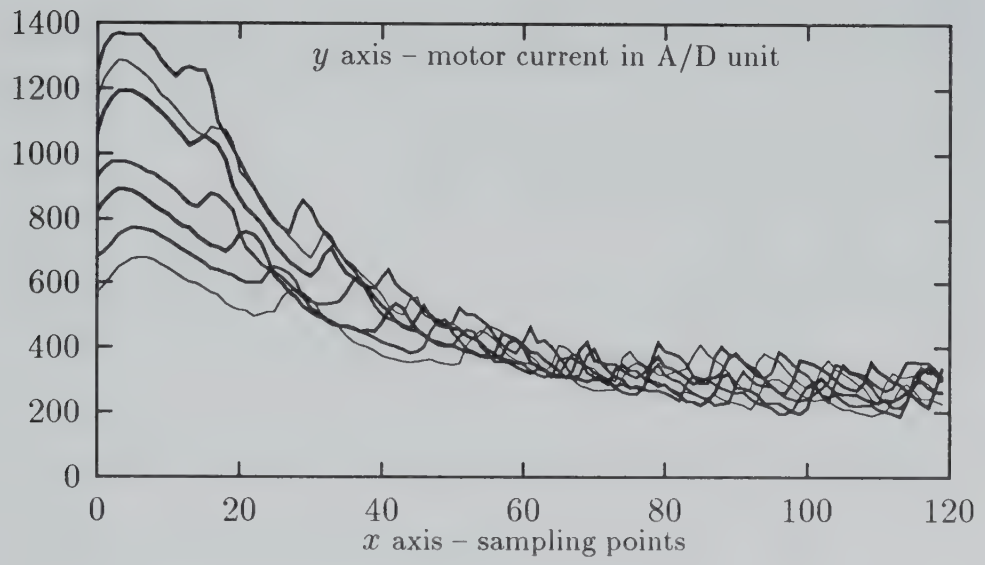


Figure 15: Current Starting Process(Counterclockwise) Under Different Voltages

| Summation in A/D unit | 6385 | 8187 | 10070 | 12132 | 12132 | 15782 | 17175 | 19143 |
|---|---|---|---|---|---|---|---|---|
| $\dot{\theta}_{final}$ | 5 | 6 | 7 | 8 | 8 | 9 | 10 | 11 |

Table 2.4: Inertia Identification in the Counterclockwise Direction

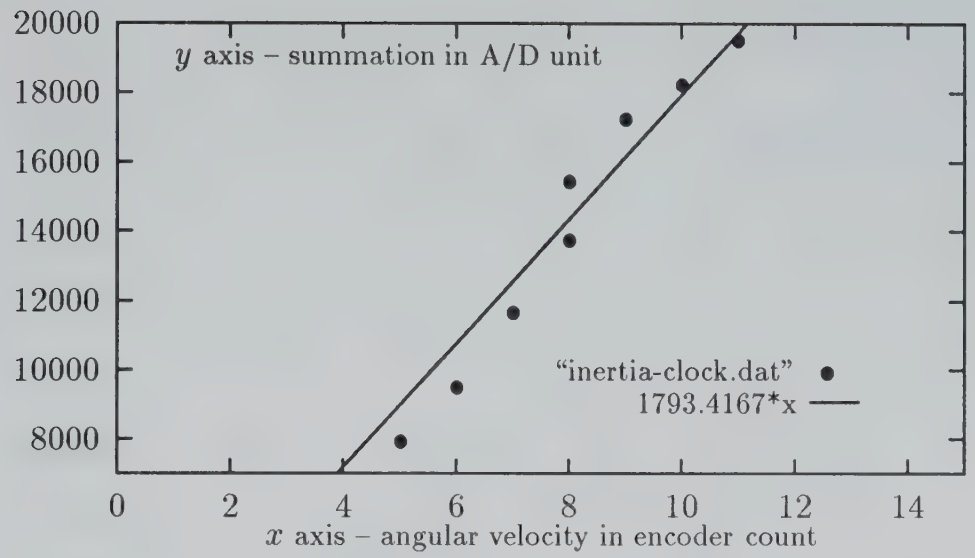


Figure 16: Least Square Solution of Motor Inertia(Clockwise)

$1611.1296 \times 1.25 \times 10^{-3} \cdot K_I = 2.0139 K_I$.

The least square solutions for both directions are shown in Figure 16 and Figure 17.

#### 2.3.2.4 Resistor $R$ and Back EMF Constant $K_{emf}$

The basic relation between the voltage applied to the armature and the current going through the windings is(neglect inductance):

$$V = R \cdot I + K_{emf} \cdot \dot{\theta} \tag{2.27}$$

If $\dot{\theta} = 0$, then the above equation becomes very simple:

$$V = R \cdot I \tag{2.28}$$

Experimental data on $V$ and $I$ for both directions are in Table 2.5 and Table 2.6.

Assume $\alpha = R$, the least square solution of equation ( 2.28) for both directions is $\alpha_{cw} = 10.3523$ and $\alpha_{ccw} = 11.2830$ in A/D unit respectively.

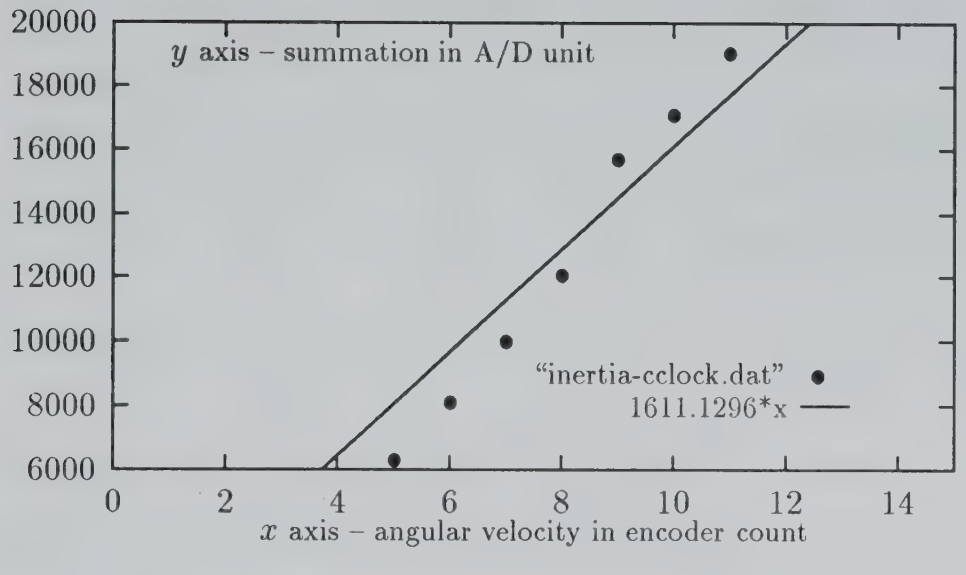


Figure 17: Least Square Solution of Motor Inertia(Counterclockwise)

| $V$(in A/D unit) | 7200 | 8200 | 9200 | 10200 | 11200 | 12200 |
|---|---|---|---|---|---|---|
| $I$(in A/D unit) | 630 | 756 | 820 | 1005 | 1130 | 1220 |

Table 2.5: Resistor Identification in the Clockwise Direction

| $V$(in A/D unit) | 7200 | 8200 | 9200 | 10200 | 11200 | 12200 |
|---|---|---|---|---|---|---|
| $I$(in A/D unit) | 590 | 630 | 830 | 900 | 1050 | 1100 |

Table 2.6: Resistor Identification in the Counterclockwise Direction

| $V - R \cdot I$ in A/D unit | 10092 | 11973 | 13853 | 15734 | 17636 | 19463 | 21311 |
|---|---|---|---|---|---|---|---|
| $\dot{\theta}$ | 14.5 | 17.5 | 21 | 24 | 27 | 30.5 | 33.5 |

Table 2.7: $K_{emf}$ Identification in the Clockwise Direction

| $V - R \cdot I$ in A/D unit | 9951 | 11951 | 13853 | 15723 | 17604 | 19408 | 21257 |
|---|---|---|---|---|---|---|---|
| $\dot{\theta}$ | 14.5 | 17.5 | 20.5 | 23.5 | 26.5 | 30 | 33 |

Table 2.8: $K_{emf}$ Identification in the Counterclockwise Direction

In order to identify $K_{emf}$, we change equation( 2.27) to be

$$V - R \cdot I = K_{emf} \cdot \dot{\theta} \tag{2.29}$$

Experimental data are again shown in Table 2.7 and Table 2.8.

The least square solution of $K_{emf}$ is therefore 654.0 and 659.57 for the clockwise and the counterclockwise direction respectively.

#### 2.3.2.5 Torque Constant $K_I$

Torque constant relates the motor current directly to the joint torque. Therefore, it is an important parameter for joint torque sensing. The basic relation is

$$\tau_j = K_I \cdot I - F \tag{2.30}$$

where $\tau_j$ is the joint torque and $F$ is the friction. $G$ is the gravity and $N$ is the inertia term. The joint torque relates to the end-point force by the direct kinematics and some bias value because of link gravity and inertia. For the single-joint robot, it becomes

$$\tau_j = F_e \cdot L + G + N \tag{2.31}$$

| $I$ in A/D unit | $F_e$ in oz | | | | Mean Value of $F_e$ |
|---|---|---|---|---|---|
| | 1st | 2nd | 3rd | 4th | |
| 200 | 7 | 7 | 7 | 7 | 7 |
| 224 | 10 | 10 | 10 | 10 | 10 |
| 233 | 11 | 10.5 | 10 | 11 | 10.625 |
| 276 | 16 | 16 | 16 | 16 | 16 |
| 302 | 20 | 19 | 20 | 20 | 19.75 |
| 328 | 22 | 23 | 23 | 23 | 22.75 |
| 354 | 25 | 26 | 26 | 26 | 25.75 |
| 389 | 30 | 30 | 30 | 30 | 30 |
| 405 | 32 | 32 | 32 | 32 | 32 |
| 431 | 35 | 35 | 35 | 35 | 35 |
| 457 | 38 | 38 | 38 | 38 | 38 |
| 483 | 40 | 41 | 40 | 41 | 40.5 |

Table 2.9: Experimental Data on Identifying Torque Constant

where $F_e$, $L$, $G$ and $N$ are end-point force acting upon the tip of the link, link length, link gravity and the inertia term respectively. When combining the above two equations, we have the following

$$F_e = K_I' \cdot I - B \tag{2.32}$$

where $K_I' = K_I/L$ and $B = (N + G + F)/L$. Because the end-point force will be used to be a comparison basis, we refer to $K_I'$ as the torque constant and $B$ as the bias value which is due to friction, gravity and inertia. In the following experiments, friction is feedforward compensated by table look-up technique. Since viscous friction is small due to low velocity, the table only consists of the Coulomb friction and torque ripples. In order to calculate the model, four separate experiments were carried out for each motor current. The experimental data are shown in Table 2.9.

Assuming $\alpha = \begin{bmatrix} K_I' \\ -B \end{bmatrix}$, it is almost routine to find out the least square solution of $\alpha$ based on equation ( 2.32). The solution is $K_I' = 0.12029$ oz of per A/D unit and

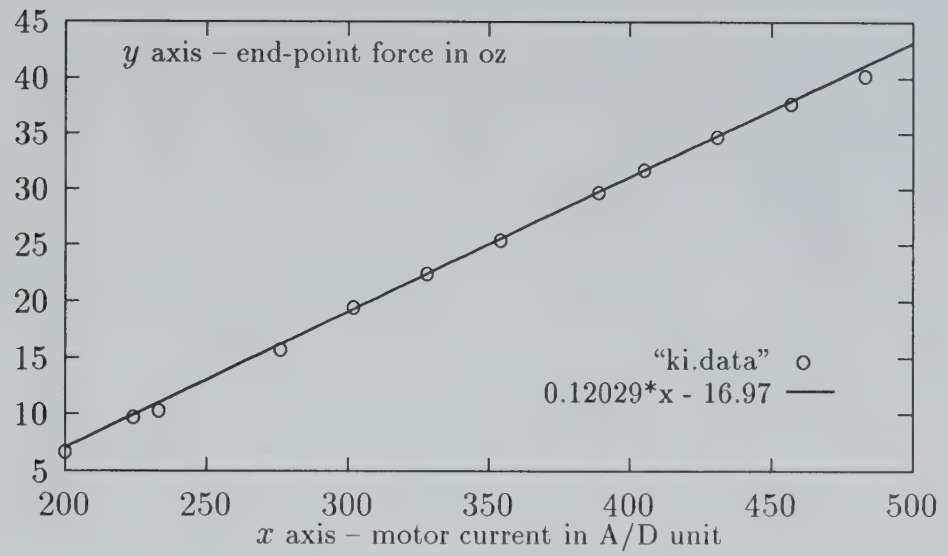


Figure 18: Linear Model of The Torque Constant

$B = 16.97$ oz. The experimental data together with its linear model are plotted in Figure 18.

#### 2.3.2.6 Force Sensitivity $K_s$

According to equation ( 2.15) and equation ( 2.16), it is clear that the strain is proportional to the applied moment which, again, is proportional to the end-point force. The strain relates the output voltage of the Wheatstone bridge by equation ( 2.5) which does not appear to be a linear relation. However, since the output voltage is so small(mili-volts) compared to the input voltage(5 volts) that the ratio $V_r$ is near zero. Therefore, equation ( 2.5) becomes

$$\varepsilon = \frac{-4V_r}{G_f} = \frac{-4}{G_f \cdot V_{in}} \cdot V_{out} \tag{2.33}$$

which is a linear relation. The force sensitivity $K_s$ is defined in the expression

$$F_e = K_s \cdot V_{out} + b \tag{2.34}$$

| $V_{out}$ in A/D unit | | | | $F_e$ in oz | | | | Mean Value of $V_{out}$ | Mean Value of $F_e$ |
|---|---|---|---|---|---|---|---|---|---|
| 1st | 2nd | 3rd | 4th | 1st | 2nd | 3rd | 4th | | |
| 740 | 700 | 670 | 660 | 7 | 7 | 7 | 7 | 692.5 | 7 |
| 980 | 980 | 920 | 930 | 10 | 10 | 10 | 10 | 952.5 | 10 |
| 1020 | 960 | 970 | 940 | 11 | 10.5 | 10 | 11 | 972.5 | 10.625 |
| 1500 | 1460 | 1460 | 1450 | 16 | 16 | 16 | 16 | 1467.5 | 16 |
| 1840 | 1750 | 1770 | 1790 | 20 | 19 | 20 | 20 | 1787.5 | 19.75 |
| 2060 | 2060 | 2050 | 2100 | 22 | 23 | 23 | 23 | 2067.5 | 22.75 |
| 2300 | 2310 | 2310 | 2290 | 25 | 26 | 26 | 26 | 2302.5 | 25.75 |
| 2680 | 2670 | 2670 | 2670 | 30 | 30 | 30 | 30 | 2672.5 | 30 |
| 2860 | 2850 | 2860 | 2830 | 32 | 32 | 32 | 32 | 2850 | 32 |
| 3140 | 3120 | 3100 | 3100 | 35 | 35 | 35 | 35 | 3115 | 35 |
| 3400 | 3350 | 3360 | 3340 | 38 | 38 | 38 | 38 | 3362.5 | 38 |
| 3640 | 3620 | 3600 | 3600 | 40 | 41 | 40 | 41 | 3615 | 40.5 |

Table 2.10: Readings Out of The Wheatstone Bridge

where $F_e$ is the end-point applied force, $V_{out}$ is the output of the Wheatstone bridge and $b$ is the bias value which may be due to the self-weight of the spring balance or/and the measurement error. Note that we set the unstrained output of the bridge to zero in the above derivations. Experimental data are recorded in Table 2.10.

Assuming $\alpha = \begin{bmatrix} K_s \\ b \end{bmatrix}$, the least square solution to equation ( 2.34) is: $\alpha = \begin{bmatrix} 0.011496 \\ -0.8246 \end{bmatrix}$ and the solution together with the linear model is shown in Figure 19.

## 2.4 Summary

We have presented some design details about a single-joint robot. Parameter identification of the single-joint robot is carried out experimentally. In a six DOF robot, the same parameters as shown in our single-joint robot have to be identified for each joint. Procedures of identification and calibration in a single-joint case can be

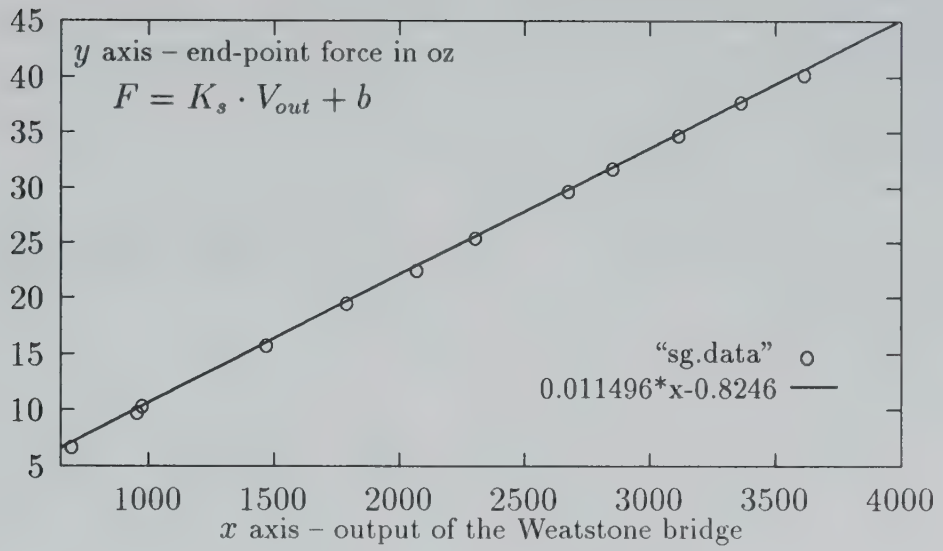


Figure 19: Least Square Solution to End-Point Force Sensitivity

extended. Wrist mounted torque/force sensor has to undergo the same calibration procedure as was taken here for the strain gauge. Torque constant for each motor can also be identified based on equations( 2.30) through ( 2.32), except direct kinematics will be complicated in a six DOF case. Friction identification will be a little difficult because it has to be carried out on-line. Some other parameters, such as motor inertia and link inertia, are also difficult to identify because of the coupling between links. However, there has been work done in this area(for example[48]).

# Chapter 3

# Sensor Data Fusion

Sensors retrieve particular properties from the environment. Sensor data fusion is the process of combining sensor input to infer a consensus view about the environment.

Any single sensor has its fundamental limitations to function as an independent knowledge source. It can only reflect the environment partially and imprecisely. Although design of powerful and reliable sensors is an interesting research topic[12], a natural alternative is to combine different sensors to infer a consensus which can not be obtained from any single sensor. Sensor data fusion can also prevent accidents by successfully detecting failure of one or more of system key sensors, an otherwise disastrous situation.

In recent years, there have been a number of studies on sensor data fusion techniques and applications, among which are: [10, 23, 43, 16, 42, 8, 34, 24, 22, 1, 28, 3, 50, 2], for example. To the concern of all researchers is the problem of characterization of sensor behavior due to facts that no sensor is perfect and the output always contains noise, be it slight or serious. The statistical model is appropriate and has been used by

most researchers. We also believe that a statistical model is proper to describe sensor behaviors in our experimental system. The following sections proceed as follows; first, we introduce the Maximum-Likelihood(ML) method which is most often used in sensor data fusion; then, we will have a brief overview of major works done in the field and provide some comments.

## 3.1 The Maximum-Likelihood Method

The maximum likelihood method[35] is a general and powerful estimation procedure. Let $Z_1, Z_2, \cdots, Z_n$ be $n$ knowledge sources at a given instance, $\theta$ be the scalar parameter to be estimated by combining these $n$ independent sources of knowledge, and $f(\cdot)$ be the probability density function. We define log likelihood function by

$$L = \log f(Z_1, Z_2, \cdots, Z_n|\theta) \tag{3.1}$$

or the logarithm of the joint conditional density of $(Z_1, Z_2, \cdots, Z_n)$ given the parameter $\theta$, even though $\theta$ is unknown. We would like to choose the most probable value of $\theta$ after each $Z_i$ is available. The *maximum likelihood cstimate*(ML) of $\theta$, $\hat{\theta}$, is given by the solution to

$$\frac{dL}{d\theta} = 0 \tag{3.2}$$

In the case of a vector parameter $\theta$, the ML estimate of each unknown parameter is obtained by solving the partial differentials of the log likelihood function with respect to each unknown parameter.

If the received values of $Z_1, Z_2, \cdots, Z_n$ are independent, the log likelihood function becomes

$$L = \log f(Z_1|\theta) + \log f(Z_2|\theta) + \cdots + \log f(Z_n|\theta) = \sum_{i=1}^{n} \log f(Z_i|\theta) \tag{3.3}$$

In the case of two sensors, assume that each sensor is independent of the other and the Gaussian distribution density of each sensor is

$$f(Z_i|\theta) = \frac{1}{\sqrt{2\pi}\sigma_i} e^{-\frac{(Z_i-\theta)^2}{2\sigma_i^2}} \quad i = 1, 2 \tag{3.4}$$

where $\sigma_i^2$ is the variance of $i$th sensor. Because of the independence assumption, the joint distribution density is simply the product of two Gaussian densities. Substitute ( 3.4) into ( 3.3) and ( 3.2), the following is obtained:

$$\hat{\theta} = \frac{\frac{Z_1}{\sigma_1^2} + \frac{Z_2}{\sigma_2^2}}{\frac{1}{\sigma_1^2} + \frac{1}{\sigma_2^2}} \tag{3.5}$$

The above equation makes physical sense since we tend to believe, and hence put more weight on the data that have less uncertainty, i.e., data with smaller $\sigma^2$. Because of its simple calculations and straightforward format, there have been many works done using this method for sensor data fusion.

Before moving on to the next section, it is important to make a few remarks on the independence assumption of the ML algorithm. This assumption is generally known as "constraints"[11], and is intended to make the problem mathematically tractable. Of course, in practical applications one may question the validity of the assumption and ask what will happen if the assumption is not true. In our case, the assumption may not be true if the noise distributions of the two sensors are dependent or if the two sensors are strongly coupled, i.e., the outputs of these two sensors are dependent. There are many techniques to decouple the correlation of noises(e.g. [35]). More seriously, if the outputs of sensors are dependent, the ML may not be applicable any longer, and some other fusion algorithms have to be developed(typically, adaptation algorithms are involved). In the context of sensor data fusion, reference[11] deals with the dependence problem of sensor outputs more systematically. For example, the authors consider the case when each of the two or more sensors can produce a

unique solution to the problem examined as sensor working independently. The only purpose of sensor data fusion in this case is to reduce the uncertainty of the resulting fused value. Our proposed joint torque sensing scheme is quite similar to this case. As a result, we will assume independence of the two sensors in the later chapters without further explanations.

## 3.2 An Overview of Sensor Data Fusion

There have been some survey works done recently, for example[22]. However, they are not necessarily complete since some topics are not covered. We will list some major works done in the field, and try to classify their ideas, strategies, results and contributions.

Richardson and Marsh[42] studied both conceptual and applied sensor data fusion methodology. They concluded in the conceptual part that the fusionability of various kinds of raw data from different sensors requires that each sensor has to have stand-alone significance. In the applied part, they actually used the maximum *a posteriori* estimator to combine TV camera images and acoustical measurements to determine the geometry(elevation function) of an object resting upon a flat surface. Ayache and Faugeras[8] dealt with the problem of building three-dimensional descriptions of the environment of a mobile robot using passive vision. It is shown that visual maps corresponding to different positions of the robot can be registered to compute an accurate estimate of its displacement between the various viewpoint positions, assuming an otherwise static environment. They proposed to build, register and fuse visual maps within the general framework of extended Kalman filter. Durrant-Whyte[16] has presented a theory and methodology for integrating and propagating geometric

sensor observations to obtain knowledge about an uncertain geometric environment. The method is based on the Bayesian techniques and on statistical decision theory, and is applicable to general sensors with Bayesian model as a basis. Hashimoto and Paul[28] proposed a method to combine redundant joint state(position and velocity) information to provide a robust robot control strategy. The idea is that joints equipped with both position and velocity sensors(encoder and tachometer) are considered sensor redundant since by differentiating joint position of a robot, velocity is obtained, and by integrating velocity, position is also obtained. The redundant sensor information is then shown to detect a sensor failure, a catastrophic situation which can not be dealt with effectively in a sensor non-redundant system. The actual state of the system(position and velocity) was obtained by combining information from both sensors using a Minimum Variance estimate which is the General Least Square estimate with the weight matrix substituted by the inverse of sensor variance matrix. A cross-checking hypothesis test is also performed to monitor the condition of the control system.

The integration of multiple sensors into an existing intelligent control system is also an important aspect of sensor data fusion. Luo, Lin and Scherp[34] studied the method of developing an intelligent robot system via the integration of multiple sensors into robot tasks. They studied the way in which to integrate a set of data observed from two or more sensors into a consensus using probability curves to define "distance matrix" and analyze "confidence distance measures". Abidi and Gonzalez[2] showed how to utilize different sensors at different stages to perform two space tasks. Their experiment robot is equipped with vision, range, sound, proximity, touch and force/torque sensors. Zheng[50] proposed an evaluation strategy for an intelligent system based on multisensor integration. He also suggested that the concept of logical sensor is most suitable for the multisensor integration into an intelligent system. A logical sensor is

a data abstraction which consists of a collection of information and a set of operations defined about the information. The information could be raw data extracted by an individual sensor, or new knowledge inferred from a combination of sensor data. By communicating and manipulating the information collected by logical sensors, multiple sensors can be hierarchically integrated into a system.

Many papers were also published on the study of combination of quite different kinds of sensors, such as camera and tactile sensor, camera and acoustical sensor etc. for object recognition. These papers study the heuristics for particular applications to bring different sources of information together rather than studying data fusion strategies and therefore are difficult to extend consistently to general sensors. A typical example is seen in[3]. Also, a number of other issues have been studied, among them are: sensor data fusion on a parallel processor[10], sensor data fusion through a distributed blackboard[23], and sensor data fusion to provide flexible control strategies[43].

## 3.3 Summary

In this chapter, we discussed sensor data fusion in general. The ML method was presented in detail. Some major works on sensor data fusion were overviewed.

It should be noted that in real applications, one may turn to different fusion algorithms. Kalman filter technique is a powerful tool to deal with dynamic systems with large amount of noises. Some other techniques such as the Bayesian method can also be used.

# Chapter 4

# Joint Torque Sensing Based On Sensor Data Fusion

The method we proposed to sense joint torque is to combine motor currents and wrist mounted torque/force sensor. In a single-joint robot, the wrist mounted torque/force sensor is referred to as the end-point force sensor. In our experiment system, this sensor consists of a strain gauge and its electronics to measure the force acting on the tip of the link. In this chapter, we focus on our experimental system and describe how to obtain the actual joint torque and what those factors are that could contribute to sensor uncertainties. We also provide a framework to analyze sensor data error and to derive statistical *a priori* knowledge. An evaluation procedure of sensor data fusion is proposed. Finally, we will discuss extending the work to a six DOF robot in general.

## 4.1 Actual Joint Torque

Actual joint torque refers to the actual torque on the reducer shaft. The conventional way to obtain this torque is to mount a set of strain gauges on the shaft and undertake the calibration work. In a single joint system, an easy way is to derive the joint torque from the end-point force acting on the tip of the link provided that there is not much uncertainty between the tip-of-link and the shaft.

We note that the joint torque is related to the end-point force by equation( 2.32) which is written here again

$$\tau_j = F_e \cdot L + G + N$$

where $\tau_j$ is the joint torque on the reducer shaft, $F_e$ is the end-point force acting on the tip-of-link, $L$ is the link length and $G$ and $N$ are torques introduced by link gravity and link inertia. Since gravity is a constant once the link is designed, and since there is no dynamics if we only consider the static case in which the joint is stationary, joint torque can be derived from the end-point force and the end-point force can be used as a comparison basis.

## 4.2 Motor Current Derived Joint Torque

It is common knowledge that output torque of a motor is proportional to the electric current going through rotor windings. Hence, by manipulating motor current, we should be able to achieve the desired joint torque applied by the motor. It has been attempted in DDArm systems[20, 36, 7]. However, it becomes complicated when there is a reducer in the arm system, such as in our system. As we have seen in

Chapter 2, the relation between motor current and joint torque is as follows

$$\tau = K_I \cdot I - F \tag{4.1}$$

where $F$ is the torque loss because of friction. It is clear from this equation that the accuracy of obtaining joint torque from motor current is subject to three factors: torque constant $K_I$, motor current $I$ itself and friction $F$. In a strict sense, $K_I$ is nonlinear, and the degree of the nonlinearity varies with the type and the structure of the motor. Many factors, such as commutation error, stiction and magnetic flux saturation, may contribute to the torque constant nonlinearity[20]. Linearization is possible through the direct feedback of joint torque by a shaft-mounted torque sensor[49, 7]. Other methods are also attempted by some researchers. Table look-up technique was used to compensate the nonlinearity of torque constant in [20], where the steady state joint torque was recorded in a two dimension matrix with respect to motor current and position. A linearizing commutation algorithm was developed in [36] to adjust the motor current dynamically as it goes through each phase(base current as it is called). Torque output is studied via different profile of base current(default commutation profile). However, these described methods were applied to DDArm systems, where very little friction exists to affect the system performance. In our experiment system, there are two other major factors to affect the nonlinearity of the torque-current relationship, namely friction introduced mainly by the reducer and the inability to control motor current accurately due to hardware limitations. Measurement noise caused by the A/D converter may also contribute to the nonlinear relation, though the magnitude may be small. Hence, it is reasonable to assume that $K_I$ in equation( 4.1) can be taken as a constant. Instead of identifying torque constant $K_I$ directly, we formulated and identified in Chapter 2 the constant that relates motor current and the end-point force, as it was termed $K_I'$ in equation( 2.32). The way

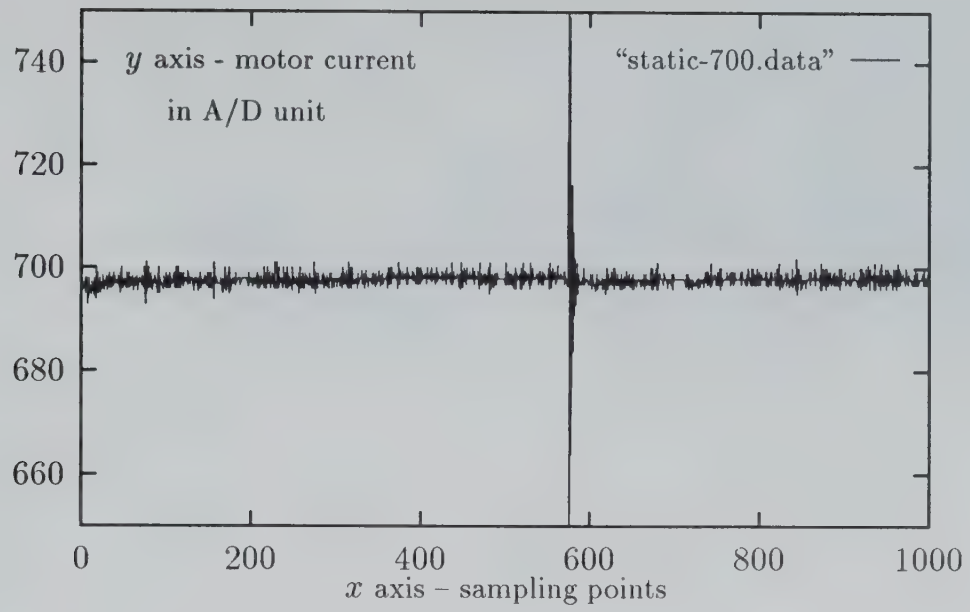


Figure 20: Current Profile in Static Case, Desired Value is 700

that we control motor current is shown in equation( 2.27) and can be rewritten here.

$$V = R \cdot I + K_{emf} \cdot \dot{\theta}$$

Note that we neglect inductance of rotor windings which could also introduce uncertainty in the control of motor current. The resistor $R$ might change slightly with the ambient temperature to add extra noise to the current measurement. More seriously, the back emf constant $K_{emf}$ has almost the same property as torque constant $K_I$ and this means that nonlinearity of $K_{emf}$ will introduce difficulties to control the motor current. Figure 20 and Figure 21 show the current profile using parameters identified in Chapter 2 in the case of $\dot{\theta} = 0$(static case) and in the case of $\dot{\theta} \neq 0$(dynamic case) respectively. In both cases, the desired current value is a constant. We can clearly see that in the dynamic case, more noise is associated with each reading due to a combination of factors stated above.

Since we can always improve the system hardware, such as implementing a current servo, to make motor current more accurate and less noisy, we consider friction as

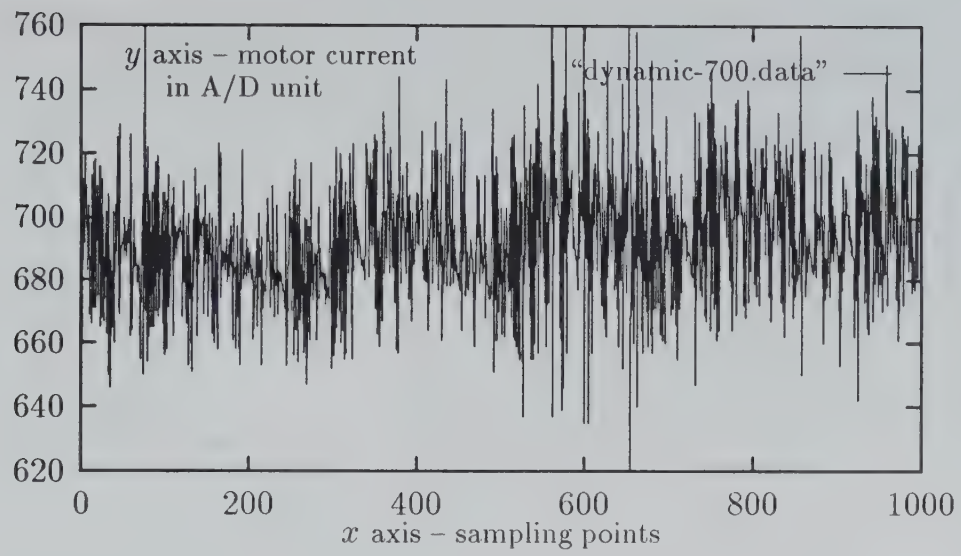


Figure 21: Current Profile in Dynamic Case, Desired Value is 700

the only error source that contaminates the accuracy of measurements. In order to emphasize the disturbance effect of the friction, we only study the static case because the motor current is more stable than that in the dynamic case, as can be seen from Figure 20 and Figure 21. Also, we study the static case to facilitate the measurement of the end-point force, because the end-point force will be used to serve as a comparison basis. An error analysis based on equation( 2.32) for the motor current sensor in the static case will be carried out next, and the statistical *a priori* knowledge of the sensor will be derived accordingly.

The same procedure that was used to identify $K_I'$ is taken again. The following table contains the experimental data. For each desired value of the end-point force, five independent experiments were carried out. The error between the desired value and the actual value is calculated and shown in Table 4.11 together with the data.

It is well-known that the variance of $n$ samples with each element $X_i$ is calculated as

| Model Value(oz) | $F_e$ Actual(oz) | | | | | Error | | | | | Variance |
|---|---|---|---|---|---|---|---|---|---|---|---|
| | 1st | 2nd | 3rd | 4th | 5th | 1st | 2nd | 3rd | 4th | 5th | |
| 1.1 | 3 | 1 | 0 | 0 | 1 | -1.9 | 0.1 | 1.1 | 1.1 | 0.1 | 1.5125 |
| 4.1 | 4 | 4 | 4 | 4 | 4 | 0.1 | 0.1 | 0.1 | 0.1 | 0.1 | 0.0125 |
| 5.3 | 4.5 | 6 | 4.5 | 6 | 6 | 0.9 | -0.7 | 0.9 | -0.7 | -0.7 | 0.795 |
| 8.3 | 8.5 | 8 | 8.5 | 8.5 | 8 | -0.2 | 0.3 | -0.2 | -0.2 | 0.3 | 0.075 |
| 11.3 | 10 | 9.5 | 11.5 | 10 | 9.5 | 1.3 | 1.8 | -0.2 | 1.3 | 1.8 | 2.475 |
| 14.3 | 14.5 | 14 | 14 | 14 | 14 | -0.2 | 0.3 | 0.3 | 0.3 | 0.3 | 0.1 |
| 17.3 | 17 | 17.5 | 17.5 | 18 | 17.5 | 0.3 | -0.2 | -0.2 | -0.7 | -0.2 | 0.175 |
| 20.3 | 20.5 | 20.5 | 20 | 21 | 20.5 | -0.2 | -0.2 | 0.3 | -0.7 | -0.2 | 0.175 |
| 23.4 | 24 | 24 | 24 | 24 | 24 | -0.6 | -0.6 | -0.6 | -0.6 | -0.6 | 0.45 |
| 26.3 | 26 | 26 | 26 | 27.5 | 27 | 0.3 | 0.3 | 0.3 | -1.2 | -0.7 | 0.55 |
| 29.6 | 29.5 | 30 | 30 | 31 | 30.5 | 0.1 | -0.4 | -0.4 | -1.4 | -0.9 | 0.775 |
| 32.6 | 32.5 | 32.5 | 33 | 33.5 | 34 | 0.1 | 0.1 | -0.4 | -0.9 | -1.4 | 0.7375 |
| 35.6 | 35.5 | 36 | 36 | 36 | 36 | 0.1 | -0.4 | -0.4 | -0.4 | -0.4 | 0.1625 |

Table 4.11: Motor Current Data Used for Deriving Statistics

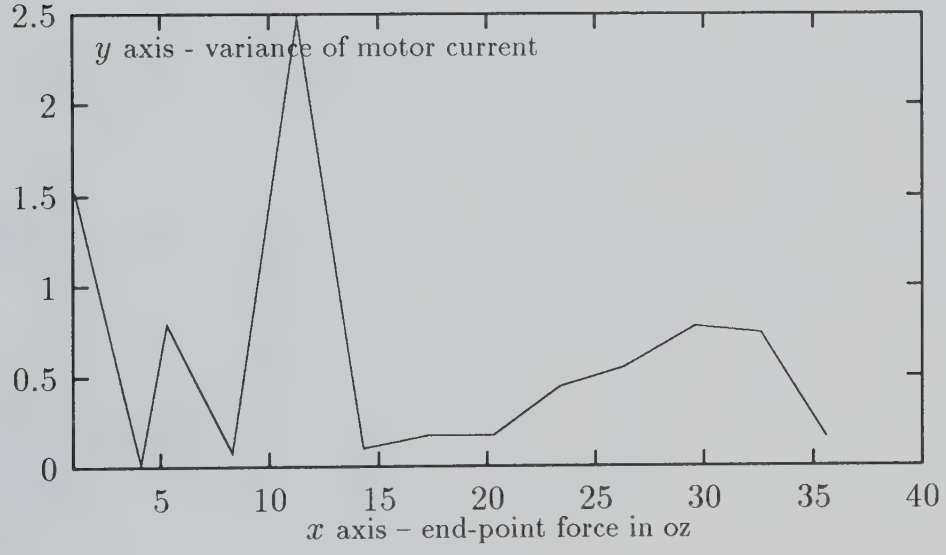


Figure 22: Variance Plot of Motor Current

follows

$$\sigma^2 = \frac{1}{n-1}\sum_{i=1}^{n}(X_i - \overline{X})^2 \tag{4.2}$$

where $\overline{X}$ is the mean of samples. Assume $X_i$ represents each $F_e$ in Table 4.11 and $\overline{X}$ is the modeled value, the above equation becomes

$$\sigma^2 = \frac{1}{4}\sum_{i=1}^{5} e_i^2 \tag{4.3}$$

where $e_i$ is the error shown in Table 4.11. The calculated variances corresponding to different desired end-point forces are shown in Table 4.11. The variances are also plotted with respect to the end-point force in Figure 22. It should be noted that this plot shows actually the fusion weight of motor current in the specified range of the end-point force. We can see from the figure that when the end-pint force is comparable to friction in magnitude, the variance appears uncertain and big. It is due to the nature of friction. Also, the variance decreases with the increasing of the end-point force. This means that the fusion weight of motor current becomes bigger with the increasing of the end-point force.

## 4.3 Strain Gauge Derived Joint Torque

A Wheatstone bridge which consists of a strain gauge and its electronics is mounted at the tip of the link to measure the end-point force. The output of the Wheatstone bridge is related to the end-point force by the force sensitivity equation( 2.34). The identification of force sensitivity is carried out in Chapter 2. Here we will perform an error analysis for the strain gauge sensor and derive its statistical *a priori* knowledge.

Figure 23 shows the actual readings from the strain gauge circuit. The noise is mainly caused by the A/D converter. A simple low-pass filter/smoother will remove the noise, such as the one shown in Figure 24 where a Kalman smoother is employed.

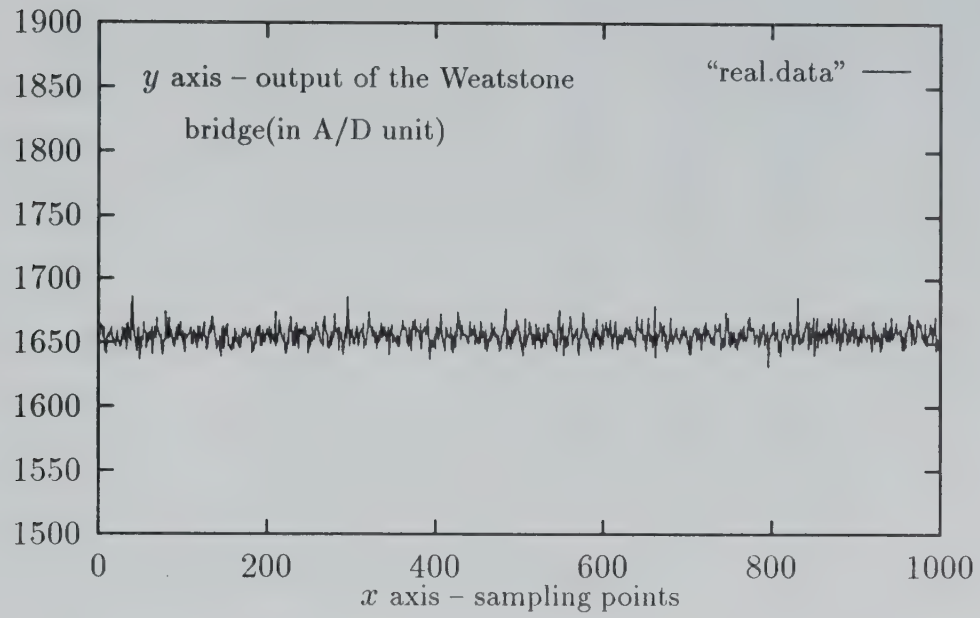


Figure 23: Readings Out of the Wheatstone Bridge

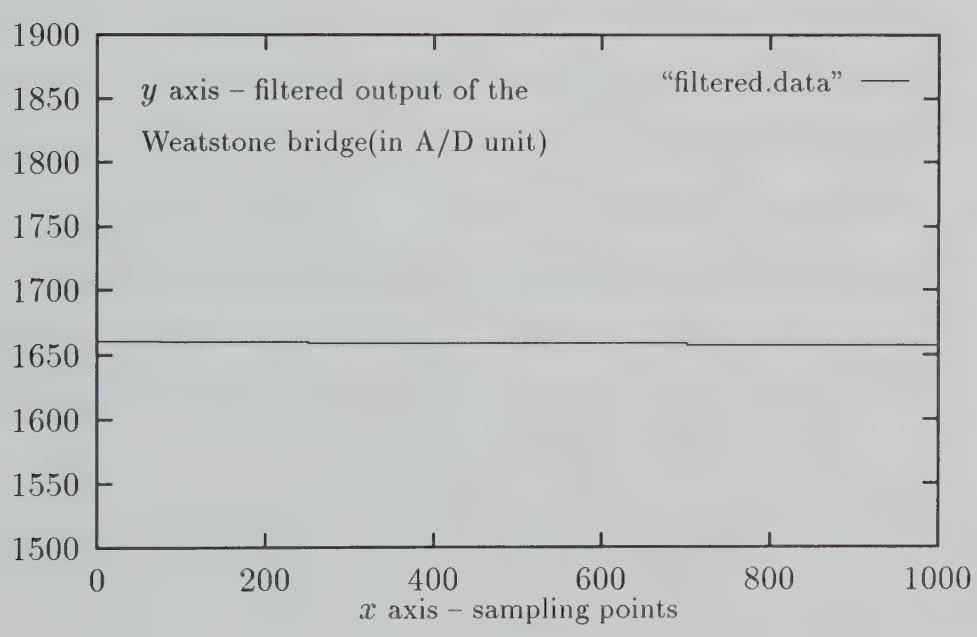


Figure 24: Low-pass Filtered Output

| $F_e$(oz) Actual | $V_{out}$(A/D unit) | | | |
|---|---|---|---|---|
| | 1st | 2nd | 3rd | 4th |
| 1 | 210 | 180 | 210 | 250 |
| 4 | 540 | 520 | 540 | 500 |
| 6 | 650 | 700 | 600 | 670 |
| 10 | 1080 | 980 | 980 | 930 |
| 14 | 1280 | 1400 | 1390 | 1340 |
| 16 | 1500 | 1460 | 1460 | 1450 |
| 18 | 1610 | 1550 | 1660 | 1600 |
| 23 | 2060 | 2060 | 2050 | 2100 |
| 24 | 2080 | 2200 | 2120 | 2070 |
| 26 | 2300 | 2310 | 2290 | 2300 |
| 30 | 2680 | 2670 | 2670 | 2700 |
| 32 | 2880 | 2860 | 2850 | 2860 |
| 35 | 3110 | 3120 | 3140 | 3130 |

Table 4.12: Strain Gauge Readings for Deriving Statistics

Experimental data of the Wheatstone bridge output are recorded in Table 4.12. The data are converted to the end-point force using the model identified in Chapter 2 and shown in Table 4.13. It is easy to calculate the error between the actual end-point force and each derived end-point force. The variances of these errors corresponding to different applied end-point forces are also calculated and shown in the table. Figure 25 shows the variance changing with respect to the end-point force. This plot will be used as the fusion weight of the strain gauge sensor within the specified range of the end-point force. It is seen that the variance also decreases with the increasing of the end-point force. The big value of variance in low range of the end-point force is believed to be caused by the uneven strain distribution upon the surface of the extra metal.

| $F_e$(oz) | Derived Value(oz) | | | | Error | | | | Variance |
|---|---|---|---|---|---|---|---|---|---|
| Actual | 1st | 2nd | 3rd | 4th | 1st | 2nd | 3rd | 4th | |
| 1 | 1.6 | 1.2 | 1.6 | 2.0 | -0.6 | -0.2 | -0.6 | -1.0 | 0.587 |
| 4 | 5.4 | 5.1 | 5.4 | 4.9 | -1.4 | -1.1 | -1.4 | -0.9 | 1.98 |
| 6 | 6.6 | 7.2 | 6.1 | 6.9 | -0.6 | -1.2 | -0.1 | -0.9 | 0.873 |
| 10 | 11.6 | 10.4 | 10.4 | 9.9 | -1.6 | -0.4 | -0.4 | 0.1 | 0.963 |
| 14 | 13.9 | 15.3 | 15.1 | 14.6 | 0.1 | -1.3 | -0.1 | -0.6 | 0.69 |
| 16 | 16.4 | 15.9 | 15.9 | 15.8 | -0.4 | 0.1 | 0.1 | 0.2 | 0.073 |
| 18 | 17.7 | 17.0 | 18.3 | 17.6 | 0.3 | 1.0 | -0.3 | 0.4 | 0.446 |
| 23 | 22.8 | 22.8 | 22.7 | 23.3 | 0.2 | 0.2 | 0.3 | -0.3 | 0.086 |
| 24 | 23.1 | 24.5 | 23.5 | 23 | 0.9 | -0.5 | 0.5 | 1.0 | 0.686 |
| 26 | 25.6 | 25.7 | 25.5 | 25.6 | 0.4 | 0.3 | 0.5 | 0.4 | 0.22 |
| 30 | 30 | 29.9 | 29.9 | 30.2 | 0 | 0.1 | 0.1 | -0.2 | 0.02 |
| 32 | 32.3 | 32.1 | 31.9 | 32.1 | -0.3 | -0.1 | 0.1 | 0.1 | 0.04 |
| 35 | 34.9 | 35 | 35.3 | 35.1 | 0.1 | 0 | -0.3 | 0.1 | 0.036 |

Table 4.13: Converted Value Based on Table 4.12

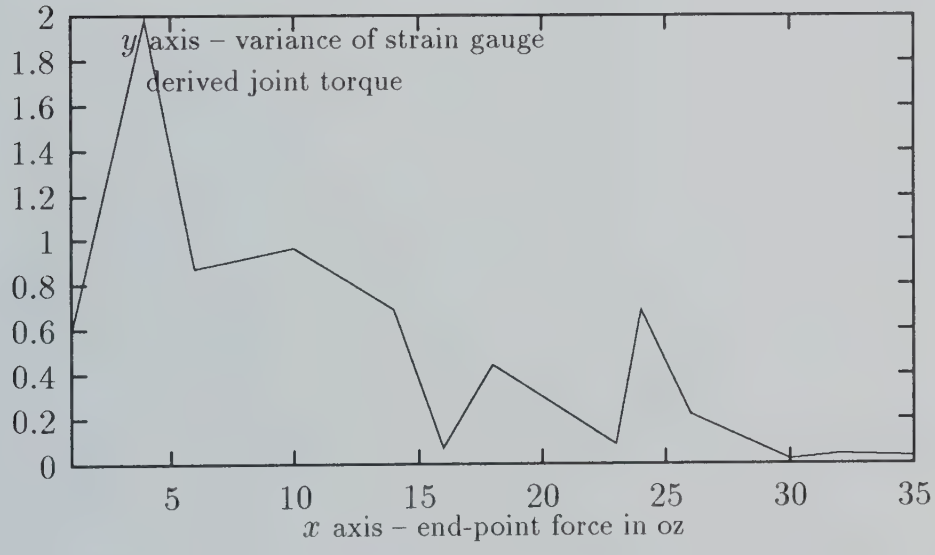


Figure 25: Variance Plot of Strain Gauge Derived Joint Torque

## 4.4 Joint Torque Sensing Based on Sensor Data Fusion

It becomes apparent from the above sections that both motor current and the end-point mounted strain gauge can retrieve joint torque indirectly. But both contain a certain amount of uncertainties. A natural way to infer an improved description of the joint torque is to combine motor current and strain gauge output or use sensor data fusion.

### 4.4.1 Fusion Algorithm

Since the statistics of both sensors are available, the Maximum-Likelihood(ML) algorithm is directly applicable. In the case of two sensors, the algorithm is known as(equation 3.5)

$$\hat{\theta} = \frac{\frac{Z_1}{\sigma_1^2} + \frac{Z_2}{\sigma_2^2}}{\frac{1}{\sigma_1^2} + \frac{1}{\sigma_2^2}}$$

where $\frac{1}{\sigma_1^2}$ and $\frac{1}{\sigma_2^2}$ are referred to the fusion weights of both sensors. We have shown how $\sigma_1^2$ and $\sigma_2^2$ are changing with respect to the end-point force in Figure 22 and Figure 25 respectively. Therefore, in combining two sensors' outputs, the fusion weight of each sensor will be changed dynamically according to the statistical *a priori* knowledge we derived earlier. The joint torque obtained in this way is believed to be more accurate than any of the two sensors. Because the weight of each sensor has to be comparable, the fusion weight of each sensor with respect to the end-point force is tuned according to the variance calculated earlier and shown in Table 4.14. Some linear interpolations between points are carried out.

| $F_e$ (oz) | $\sigma^2$ for Strain Gauge | $\sigma^2$ for Motor Current | $F_e$ (oz) | $\sigma^2$ for Strain Gauge | $\sigma^2$ for Motor Current |
|---|---|---|---|---|---|
| 1 | 0.587 | 1.5125 | 18 | 0.446 | 0.175 |
| 4 | 1.98 | 0.0125 | 20 | 0.653 | 0.175 |
| 6 | 0.873 | 0.795 | 23 | 0.086 | 0.45 |
| 8 | 0.918 | 0.075 | 24 | 0.686 | 0.45 |
| 10 | 0.963 | 1.275 | 26 | 0.22 | 0.55 |
| 12 | 0.8265 | 1.2875 | 30 | 0.02 | 0.775 |
| 14 | 0.69 | 0.1 | 32 | 0.04 | 0.7375 |
| 16 | 0.073 | 0.175 | 35 | 0.036 | 0.1625 |

Table 4.14: Fusion Weights for Both Sensors

### 4.4.2 Fusion Evaluation

Having derived fusion weights for both sensors with respect to the end-point force, we wonder how good the fusion algorithm performs under all known statistical *a priori* knowledge. In the process of deriving each sensor model we assumed the zero-mean error between sensor output and sensor model, because we can always re-calibrate the sensor if the error mean is not zero. However, in a more realistic sense, the mean can not be zero because, first, the number of samples is limited, and second, the deterministic model is not sufficient to characterize the sensor behavior and the model itself may be changing slightly. Therefore, we consider that two parameters, *mean error square*($\overline{e^2}$) and *error variance*($\sigma^2$), are important to evaluate the performance of sensor data fusion. $\overline{e^2}$ is intended to characterize how far each sensor deviates from its mathematical description, and $\sigma^2$ is the measure of convergence of sensor error. It is certainly desired for sensor data fusion to have both smaller $\overline{e^2}$ and $\sigma^2$ compared to each independent sensor. However, in the case of big $\overline{e^2}$, the comparison of $\sigma^2$ may not make sense because of the serious bias of one or more sensors. In such cases, the comparison of $\overline{e^2}$ makes more physical sense. This will be clear in the next Chapter where we introduce unmodeled disturbances into the system.

The definition of $\overline{e^2}$ and $\sigma^2$ is as follows

$$\overline{e^2} = \frac{\sum_{i=1}^{i=n} e_i^2}{n} \tag{4.4}$$

$$\sigma^2 = \frac{1}{n-1} \sum_{i=1}^{i=n} (e_i - \overline{e}) \tag{4.5}$$

where $e_i$ is the $i$th error value, and $\overline{e}$ is the error mean. The relation between $\overline{e^2}$ and $\sigma^2$ can be derived as

$$\sigma^2 = \overline{e^2} - \overline{e}^2 \tag{4.6}$$

The error mean($\overline{e}$) will also be shown in the following evaluation tables to demonstrate its nonzero value. It also helps to calculate the $\sigma^2$ from $\overline{e^2}$ shown by equation( 4.6).

In order to perform the evaluation, two separate sets of experimental data are recorded in Table 4.15. The fusion is based on fusion weights shown in Table 4.14. In the following two tables, $e_I$,$e_{sg}$ and $e_{fusion}$ are errors between the actual end-point force and the motor current derived end-point force, the strain gauge derived end-point force, and the sensor data fusion result, respectively. The models used to derive the end-point force from motor current and strain gauge are from Chapter 2. The evaluation parameters are calculated from equation( 4.4) to equation( 4.6).

From the comparison shown in Table 4.16 and Table 4.17, we see that for the first set of data, $\sigma^2$ of $e_I$, $e_{sg}$ and $e_{fusion}$ are 0.5686, 0.6771 and 0.3277, respectively. And for the second set of data, they are 0.3947, 0.8530 and 0.2760 respectively. In both cases, the error variance of sensor data fusion is smaller than that of any one of the two sensors, in other words, the error of sensor data fusion is more convergent than that of a single sensor. It should also be noted that the sensor data fusion is the best in terms of $\overline{e^2}$ in both cases. The experimental data, therefore, confirms that sensor data fusion will outperform any single sensor, as long as some statistical *a priori* knowledge is provided for each of the sensors.

| First Set | | | Second Set | | |
|---|---|---|---|---|---|
| $F_e$ | $I$ | $V_{out}$ | $F_e$ | $I$ | $V_{out}$ |
| 2.5 | 150 | 470 | 0 | 150 | 250 |
| 6 | 175 | 760 | 4 | 175 | 730 |
| 5.5 | 185 | 750 | 6 | 185 | 740 |
| 8 | 210 | 920 | 8 | 210 | 920 |
| 9.5 | 235 | 1030 | 11 | 235 | 1140 |
| 14.5 | 260 | 1430 | 14 | 260 | 1410 |
| 17.5 | 285 | 1670 | 17 | 285 | 1640 |
| 21 | 310 | 1960 | 21 | 310 | 1940 |
| 24 | 336 | 2230 | 24 | 336 | 2200 |
| 27 | 360 | 2460 | 26 | 360 | 2360 |
| 30.5 | 387 | 2740 | 30.5 | 387 | 2750 |
| 34 | 412 | 3000 | 33.5 | 412 | 3000 |
| 36.5 | 437 | 3270 | 36.5 | 437 | 3220 |

Table 4.15: Two Sets of Data for Evaluation

| $F_e$ actual(oz) | $I$ derived(oz) | $V_{out}$ derived(oz) | Fusion (oz) | $e_I$ | $e_{sg}$ | $e_{fusion}$ |
|---|---|---|---|---|---|---|
| 2.5 | 1.1 | 4.6 | 3.6 | 1.4 | -2.1 | -1.1 |
| 6 | 4.1 | 7.9 | 5.9 | 1.9 | -1.9 | -0.1 |
| 5.5 | 5.3 | 7.8 | 6.6 | 0.2 | -2.3 | -1.1 |
| 8 | 8.3 | 9.75 | 8.4 | -0.3 | -1.75 | -0.4 |
| 9.5 | 11.3 | 11 | 11.1 | -1.8 | -0.5 | -1.6 |
| 14.5 | 14.3 | 15.6 | 14.5 | 0.2 | -1.1 | 0 |
| 17.5 | 17.3 | 18.4 | 17.6 | 0.2 | -0.9 | -0.1 |
| 21 | 20.3 | 21.7 | 21.4 | 0.7 | -0.7 | -0.4 |
| 24 | 23.4 | 24.8 | 24 | 0.7 | -0.8 | 0 |
| 27 | 26.3 | 27.5 | 27.1 | 0.7 | -0.5 | 0.1 |
| 30.5 | 29.6 | 30.7 | 30.7 | 0.9 | -0.2 | 0.2 |
| 34 | 32.6 | 33.7 | 33.7 | 1.4 | 0.3 | -0.3 |
| 36.5 | 35.6 | 36.2 | 36.2 | 0.9 | 0.3 | -0.3 |
| $\overline{e^2}$ | | | | 0.8667 | 1.5438 | 0.4269 |
| $\overline{e}$ | | | | 0.546 | -0.931 | -0.315 |
| $\sigma^2$ | | | | 0.5686 | 0.6771 | 0.3277 |

Table 4.16: Evaluation of the First Set of Data

| $F_e$ actual(oz) | $I$ derived(oz) | $V_{out}$ derived(oz) | Fusion (oz) | $e_I$ | $e_{sg}$ | $e_{fusion}$ |
|---|---|---|---|---|---|---|
| 0 | 1.1 | 2.0 | 1.7 | -1.1 | -2.0 | -1.7 |
| 4 | 4.1 | 7.6 | 4.1 | -0.1 | -3.2 | -0.1 |
| 6 | 5.3 | 7.7 | 6.4 | 0.7 | -0.3 | -0.4 |
| 8 | 8.3 | 9.75 | 8.3 | -0.3 | -1.75 | -0.3 |
| 11 | 11.3 | 12.3 | 11.8 | -0.3 | -1.3 | -0.8 |
| 14 | 14.3 | 15.4 | 14.4 | -0.3 | -1.4 | -0.4 |
| 17 | 17.3 | 18.0 | 17.5 | -0.3 | -1.0 | -0.5 |
| 21 | 20.3 | 21.5 | 20.6 | 0.7 | -0.5 | 0.4 |
| 24 | 23.4 | 24.5 | 23.8 | 0.6 | -0.5 | 0.2 |
| 26 | 26.3 | 26.3 | 26.3 | -0.3 | -0.3 | -0.3 |
| 30.5 | 29.6 | 30.8 | 30.7 | 0.9 | -0.3 | -0.2 |
| 33.5 | 32.6 | 33.7 | 33.6 | 0.9 | -0.2 | -0.1 |
| 36.5 | 35.6 | 36.2 | 36.1 | 0.9 | 0.3 | 0.4 |
| $\overline{e^2}$ | | | | 0.4184 | 1.7702 | 0.3615 |
| $\overline{e}$ | | | | 0.1538 | -0.9577 | -0.2923 |
| $\sigma^2$ | | | | 0.3947 | 0.8530 | 0.2760 |

Table 4.17: Evaluation of the Second Set of Data

### 4.4.3 Fusion Heuristics

There are many factors in the system that may increase the uncertainties of both sensors substantially. For the motor current sensor, the friction is the major factor to increase its uncertainty. It is very easy to either undercompensate or overcompensate the friction effect in the system, especially in the dynamic case. For the strain gauge derived joint torque, link dynamics can make the strain gauge readings seriously biased.

We note that the fusion result of two sensors depends on the relative value, not the absolute value, of $\sigma_1^2$ and $\sigma_2^2$ due to the normalization of the denominator in equation( 3.5). In real applications, we can always change the relative weight of each sensor in the fusion algorithm. However, we need knowledge of how to change the relative weight. In other words, we need to know which one should be increased or

decreased and how much should be changed. This is known as heuristics. The reason that we study fusion heuristics is that for any physical system there are certain properties or heuristics that are unique to the system. It is certainly desirable to combine these heuristics with algorithms to improve the results.

As has been mentioned repeatedly, friction is a major factor to disturb the joint torque derived from motor current. In the dynamic case, the effect of friction will be magnified. When velocity approaches zero, friction becomes most uncertain. On the other hand, the strain gauge derived joint torque contains little uncertainty under low velocity and acceleration because link dynamics is light. This can be implemented in the fusion algorithm by assigning more weight to the strain gauge readings when velocity is near zero. Further more, the strain gauge readings may be seriously biased when the link is in sudden acceleration or deceleration because the link dynamics in this case becomes heavy. Again, this can be implemented by assigning more weight to motor current derived joint torque. As to the problem of how much the weight should be changed, it depends on how accurately we can model a particular system.

## 4.5 Summary

In this chapter, we described how to sense joint torque by combining two sources of indirect information on our single-joint robot. Techniques used to perform error analysis for sensors are directly applicable to any sensor system. Evaluation of sensor data fusion can be extended to any number of sensors.

In a six DOF robot, motor current should be calibrated against the actual torque output. Because of many nonlinearities in controlling motor current, a current servo may be necessary. The wrist mounted torque/force sensor should be calibrated against

the applied force and the error should be analyzed and compared to that of motor currents. It is very important to bear in mind that these two sensors should be comparable with each other since fusion results depend on the relative value of variance of two sensors. Finally, fusion heuristics summarized for a single-joint robot are also applicable to a six DOF robot in general.

# Chapter 5

# Robustness of the Proposed Method to Unmodeled Disturbances

We have shown in Chapter 4 that two sensors in our system can retrieve joint torque independently but both are subject to uncertainties. From the evaluation results, we draw the conclusion that sensor data fusion performs better than any single sensor can. Basically, this shows that "two sensors are better than one"[3]. However, no disturbances have been considered so far. If the proposed method is going to be applied in a real system, both sensors are always subject to disturbances. For instances, deterministic model is not sufficient to characterize friction, and the influence of non-rigid body to the link dynamics is too complicated to be computationally acceptable. Therefore, any approximation of these factors will introduce disturbances to the system. There are many other kinds of disturbance. It is generally known that they are caused by various factors in a system for which we do not have an accurate model

to describe its behavior. For example, it is usually assumed that noise is zero-mean Gaussian. The justification of assuming Gaussian density lies in the *central limit theorem*, which states that, if $x$ is the sum of $N$ independent random quantities having nonidentical density functions, then $x$ tends to have a Gaussian density function as $N \rightarrow \infty$. In our system, we consider two kinds of disturbance, due to inaccurate models of friction and link dynamics. We assume further that both disturbances are zero mean, because we can always re-calibrate the sensor if the mean is not. Our objective in this chapter is to study the performance of sensor data fusion in terms of $\sigma^2$ and $\overline{e^2}$ discussed in last chapter when one or both of the sensors are subject to unmodeled disturbances. Simulated disturbances will be deliberately added to each measurement.

Table 5.18 consists of a collection of data which are zero mean Gaussian distributed. The standard deviation in each case is 1(i.e. these data actually have normal distribution). The reason why we choose the standard deviation of 1 is because we have obtained in Chapter 4 that both sensors in our system have a standard deviation close to 1. Therefore, disturbances added to sensor measurements have to be comparable in magnitude. Also, normal distributed numbers can be easily generated by computer library functions. In the remainder of this chapter, we will use D1, D2, D3 and D4 to denote different sets of disturbance data, as shown in Table 5.18. We choose four different sets of disturbance data to avoid possible bias that a single set of data may provide. In this chapter, we will first consider adding D1 to motor current sensor while keeping strain gauge undisturbed. Then we add D2 to strain gauge sensor and keep motor current undisturbed. Finally, we will consider adding both D3 and D4 to motor current sensor and strain gauge sensor at the same time. The performance of the sensor data fusion in each of these cases will be evaluated and tabulated. We will use the same sets of test data as shown in Table 4.15 which have been evaluated

| D1 | D2 | D3 | D4 |
|---|---|---|---|
| -0.047152 | 0.889105 | -0.193925 | 0.565576 |
| 0.058836 | -1.436488 | -0.515487 | 1.246967 |
| -0.915515 | -1.006480 | -0.342968 | -0.890196 |
| 0.891629 | 1.041256 | 0.069702 | 1.604852 |
| -2.503625 | -1.660986 | -1.537184 | 0.863181 |
| -0.796754 | -0.003389 | 0.583488 | 1.778513 |
| 1.625668 | 1.314253 | 0.205146 | 0.251998 |
| -0.526133 | -1.076662 | 1.431438 | 1.130687 |
| -0.044715 | -0.453561 | 0.463121 | -0.603874 |
| 1.509757 | 0.374781 | -0.330354 | -0.172579 |
| -2.024904 | 0.333296 | 1.361038 | 0.700693 |
| -0.289220 | 0.258395 | -0.887427 | -0.330671 |
| 0.791916 | 0.416402 | 0.901699 | 1.589135 |

Table 5.18: A Collection of Normal Distributed Disturbances

with no disturbances considered. Also, the same fusion weights are used as in Table 4.14. Fusion results will be directly compared to results obtained in Chapter 4 and some explanations of the comparison follow each section.

## 5.1 Case I: Motor Current is Disturbed by D1

In this section, we add disturbance D1 to the motor current derived joint torque and keep the strain gauge derived torque not disturbed. Evaluations are done in Table 5.19 and Table 5.20 for both sets of test data respectively. Both $\overline{e^2}$ and $\sigma^2$ obtained previously when sensors are not disturbed are also listed in Table 5.19 and Table 5.20 shown as "Old $\overline{e^2}$" and "Old $\sigma^2$". All errors are plotted in Figure 26 and Figure 27. For the first set of data, the performance of sensor data fusion is the best in terms of $\overline{e^2}$ and it is not as good as the strain gauge in terms of $\sigma^2$ because of big value of $\sigma_I^2$. For the second set of data, the performance of sensor data fusion is the best in terms of both evaluation parameters, $\overline{e^2}$ and $\sigma^2$.

| $F_e$ actual(oz) | $I$ derived(oz) | $V_{out}$ derived(oz) | Fusion (oz) | $e_I$ | $e_{sg}$ | $e_{fusion}$ |
|---|---|---|---|---|---|---|
| 2.5 | 1.053 | 4.6 | 3.66 | 1.447 | -2.1 | -1.16 |
| 6 | 4.159 | 7.9 | 4.024 | 1.841 | -1.9 | 1.976 |
| 5.5 | 4.385 | 7.8 | 4.07 | 1.115 | -2.3 | 1.43 |
| 8 | 9.19 | 9.75 | 9.15 | -1.19 | -1.75 | -1.15 |
| 9.5 | 8.8 | 11 | 9.735 | 0.7 | -0.5 | -0.235 |
| 14.5 | 13.504 | 15.6 | 13.77 | 0.996 | 1.1 | 0.73 |
| 17.5 | 19.125 | 18.4 | 18.92 | -1.625 | -0.9 | -1.42 |
| 21 | 19.774 | 21.7 | 20.18 | 1.226 | -0.7 | 0.82 |
| 24 | 23.356 | 24.8 | 23.92 | 0.644 | -0.8 | 0.08 |
| 27 | 27.809 | 27.5 | 27.56 | -0.809 | -0.5 | -0.56 |
| 30.5 | 27.58 | 30.7 | 30.6 | 2.92 | -0.2 | -0.1 |
| 34 | 32.31 | 33.7 | 33.45 | 1.69 | 0.3 | 0.55 |
| 36.5 | 36.39 | 36.2 | 36.23 | 0.11 | 0.3 | 0.27 |
| $\overline{e^2}$ | | | | 2.2107 | 1.5438 | 0.9692 |
| $\overline{e}$ | | | | 0.647 | -0.931 | -0.0947 |
| $\sigma^2$ | | | | 1.7922 | 0.6771 | 0.960 |
| Old $\overline{e^2}$ | | | | 0.8667 | 1.5438 | 0.4269 |
| Old $\sigma^2$ | | | | 0.5686 | 0.6771 | 0.3277 |

Table 5.19: Evaluation of the First Set of Data Under D1 Disturbance

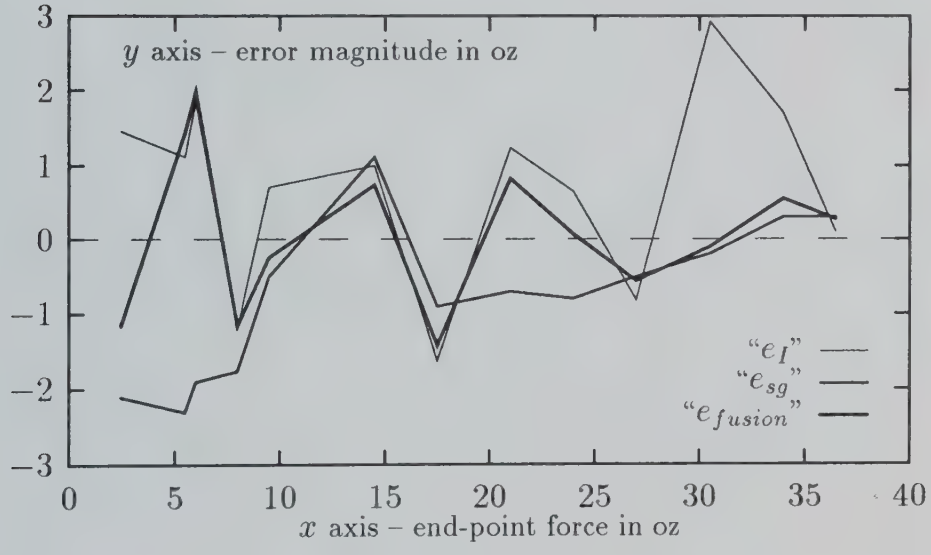


Figure 26: Error Plot of 1st Set Data When $I$ is Under D1

| $F_e$ actual(oz) | $I$ derived(oz) | $V_{out}$ derived(oz) | Fusion (oz) | $e_I$ | $e_{sg}$ | $e_{fusion}$ |
|---|---|---|---|---|---|---|
| 0 | 1.053 | 2.0 | 1.736 | -1.053 | -2.0 | -1.736 |
| 4 | 4.159 | 7.6 | 4.159 | -0.159 | -3.2 | -0.159 |
| 6 | 4.385 | 7.7 | 5.964 | 1.615 | -0.3 | 0.096 |
| 8 | 9.192 | 9.75 | 9.895 | -1.192 | -1.75 | -1.895 |
| 11 | 8.796 | 12.3 | 10.792 | 2.204 | -1.3 | 0.208 |
| 14 | 13.503 | 15.4 | 13.743 | 0.497 | -1.4 | 0.257 |
| 17 | 18.926 | 18.0 | 18.268 | -1.926 | -1.0 | -1.286 |
| 21 | 19.774 | 21.5 | 20.361 | 1.226 | -0.5 | 0.639 |
| 24 | 23.355 | 24.5 | 23.805 | 0.645 | -0.5 | 0.195 |
| 26 | 27.809 | 26.3 | 26.706 | -1.809 | -0.3 | -0.706 |
| 30.5 | 27.576 | 30.8 | 30.724 | 2.924 | -0.3 | 0.224 |
| 33.5 | 32.311 | 33.7 | 33.591 | 1.189 | -0.2 | -0.091 |
| 36.5 | 36.392 | 36.2 | 36.233 | 0.108 | 0.3 | 0.267 |
| $\overline{e^2}$ | | | | 2.2521 | 1.7702 | 0.7289 |
| $\bar{e}$ | | | | 0.3284 | -0.9577 | -0.3067 |
| $\sigma^2$ | | | | 2.1441 | 0.8530 | 0.6349 |
| $\overline{e^2}$ | | | | 0.4184 | 1.7702 | 0.3615 |
| Old $\sigma^2$ | | | | 0.3947 | 0.8530 | 0.2760 |

Table 5.20: Evaluation of the Second Set of Data Under D1 Disturbance

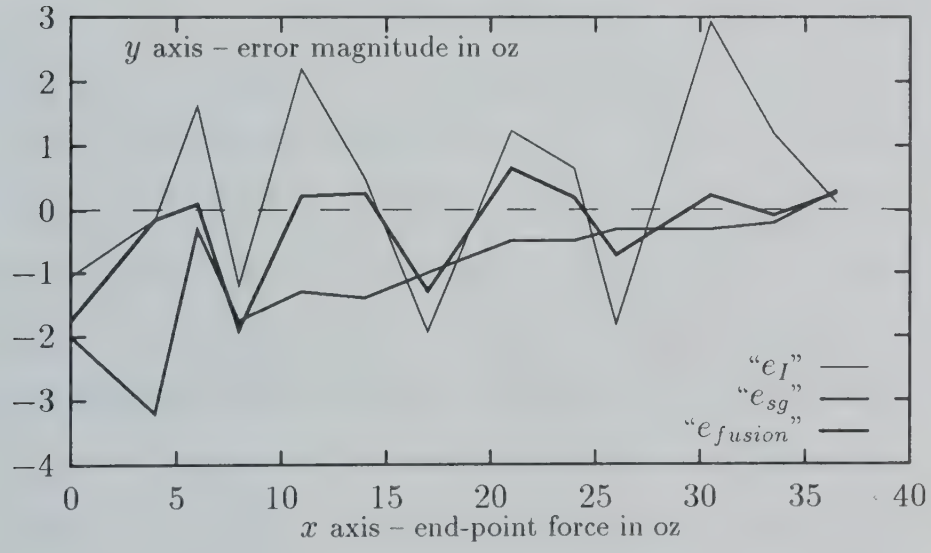


Figure 27: Error Plot of 2nd Set Data When $I$ is Under D1

| $F_e$ actual(oz) | $I$ derived(oz) | $V_{out}$ derived(oz) | Fusion (oz) | $e_I$ | $e_{sg}$ | $e_{fusion}$ |
|---|---|---|---|---|---|---|
| 2.5 | 1.1 | 5.489 | 4.263 | 1.4 | -2.989 | -2.123 |
| 6 | 4.1 | 6.464 | 5.225 | 1.9 | -0.464 | 0.775 |
| 5.5 | 5.3 | 6.794 | 6.096 | 0.2 | -1.29 | -0.596 |
| 8 | 8.3 | 10.791 | 8.483 | -0.3 | -2.791 | -0.483 |
| 9.5 | 11.3 | 9.34 | 10.183 | -1.8 | 0.16 | -0.683 |
| 14.5 | 14.3 | 15.597 | 14.464 | 0.2 | -1.079 | 0.036 |
| 17.5 | 17.3 | 19.714 | 17.98 | 0.2 | -2.214 | -0.48 |
| 21 | 20.3 | 20.623 | 20.336 | 0.7 | 0.377 | 0.664 |
| 24 | 23.4 | 24.346 | 23.771 | 0.7 | -0.346 | 0.229 |
| 27 | 26.3 | 27.874 | 27.40 | 0.7 | -0.874 | -0.4 |
| 30.5 | 29.6 | 31.033 | 31.0 | 0.9 | -0.533 | -0.5 |
| 34 | 32.6 | 33.958 | 33.85 | 1.4 | 0.042 | 0.15 |
| 36.5 | 35.6 | 36.616 | 36.43 | 0.9 | -0.116 | 0.07 |
| $\overline{e^2}$ | | | | 0.8667 | 2.0001 | 0.5630 |
| $\overline{e}$ | | | | 0.546 | -0.932 | -0.257 |
| $\sigma^2$ | | | | 0.5686 | 1.069 | 0.497 |
| Old $\overline{e^2}$ | | | | 0.8667 | 1.5438 | 0.4269 |
| Old $\sigma^2$ | | | | 0.5686 | 0.6771 | 0.3277 |

Table 5.21: Evaluation of the First Set of Data Under D2 Disturbance

## 5.2 Case II: Strain Gauge is Disturbed by D2

In this section, we consider the strain gauge derived joint torque is disturbed by D2 and the motor current derived torque not disturbed. Both sets of test data are evaluated in Table 5.21 and Table 5.22 respectively. Errors are again shown graphically in Figure 28 and Figure 29. It is not difficult to find that for the first set of test data, the performance of sensor data fusion is the best in terms of both parameters while for the second set of test data, the performance of sensor data fusion is not as good as that of motor current in terms of both parameters. This is caused by two factors. First, the noise added to the strain gauge sensor makes the sensor ill-behaved. Second, the strain gauge sensor itself deviates from its model too much, as can be seen from Figure 29.

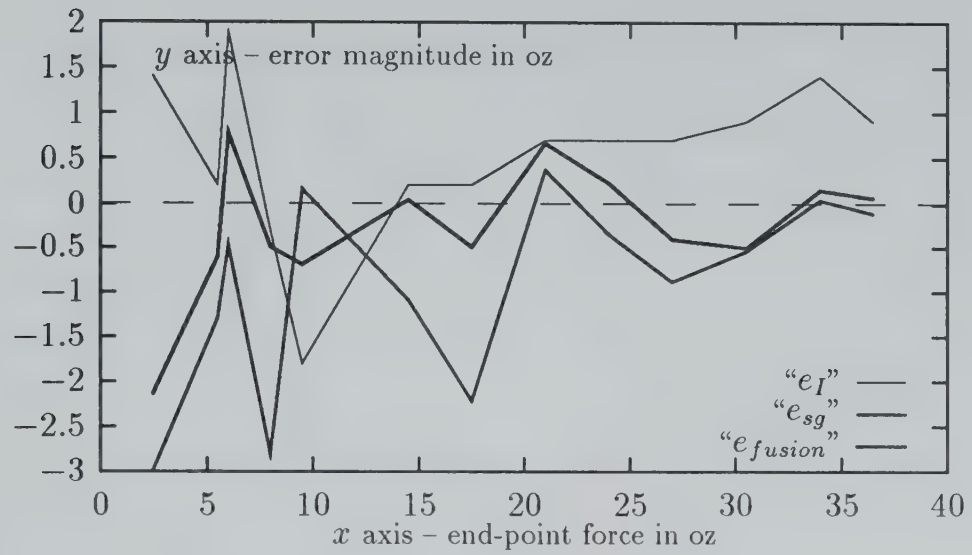


Figure 28: Error Plot of 1st Set Data When $V_{out}$ is Under D2

| $F_e$ actual(oz) | $I$ derived(oz) | $V_{out}$ derived(oz) | Fusion (oz) | $e_I$ | $e_{sg}$ | $e_{fusion}$ |
|---|---|---|---|---|---|---|
| 0 | 1.1 | 2.889 | 2.385 | -1.1 | -2.889 | -2.385 |
| 4 | 4.1 | 6.164 | 4.106 | -0.1 | -2.164 | -0.106 |
| 6 | 5.3 | 6.694 | 5.963 | 0.7 | -0.694 | 0.037 |
| 8 | 8.3 | 10.791 | 8.405 | -0.3 | -2.791 | -0.405 |
| 11 | 11.3 | 10.639 | 10.923 | -0.3 | 0.361 | 0.077 |
| 14 | 14.3 | 15.397 | 14.438 | -0.3 | -1.397 | -0.438 |
| 17 | 17.3 | 19.314 | 17.867 | -0.3 | -2.314 | -0.867 |
| 21 | 20.3 | 20.424 | 20.324 | 0.7 | 0.576 | 0.676 |
| 24 | 23.4 | 24.047 | 23.653 | 0.6 | -0.047 | 0.347 |
| 26 | 26.3 | 26.675 | 26.544 | -0.3 | -0.675 | -0.544 |
| 30.5 | 29.6 | 31.133 | 31.099 | 0.9 | -0.633 | -0.599 |
| 33.5 | 32.6 | 33.958 | 33.850 | 0.9 | -0.458 | -0.3 |
| 36.5 | 35.6 | 36.616 | 36.430 | 0.9 | -0.116 | 0.070 |
| $\overline{e^2}$ | | | | 0.4184 | 2.3192 | 0.6262 |
| $\overline{e}$ | | | | 0.1538 | -1.0185 | -0.3521 |
| $\sigma^2$ | | | | 0.3947 | 1.2819 | 0.5022 |
| Old $\overline{e^2}$ | | | | 0.4184 | 1.7702 | 0.3615 |
| Old $\sigma^2$ | | | | 0.3947 | 0.8530 | 0.2760 |

Table 5.22: Evaluation of the Second Set of Data Under D2 Disturbance

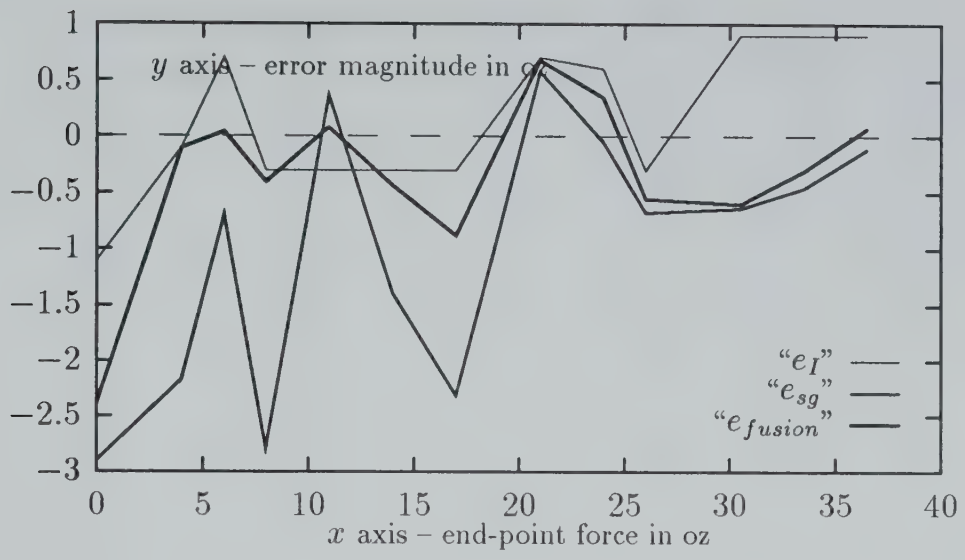


Figure 29: Error Plot of 2nd Set Data When $V_{out}$ is Under D2

## 5.3 Case III: Both Sensors are Under Disturbances

In this section, both sensors are disturbed. The motor current derived joint torque is disturbed by D3 and the strain gauge derived joint torque is disturbed by D4. Again, we take the same procedure to evaluate both sets of test data which is shown in Table 5.23 and Table 5.24 respectively. Newly derived parameters are also compared to the old ones obtained under no disturbances. Errors are also plotted in Figure 30 and Figure 31. For the first set of test data, the performance improvement of sensor data fusion is dramatic in terms of both evaluation parameters. Although both sensors are under serious disturbances, sensor data fusion seems not being affected very much. For the second set of test data, the performance of sensor data fusion is the best in terms of error variance while slightly worse than that of motor current in terms of mean error square. Considering the magnitude of each $\overline{e^2}$, we can still say that sensor data fusion outperforms each independent sensor.

| $F_e$ actual(oz) | $I$ derived(oz) | $V_{out}$ derived(oz) | Fusion (oz) | $e_I$ | $e_{sg}$ | $e_{fusion}$ |
|---|---|---|---|---|---|---|
| 2.5 | 0.906 | 5.165 | 3.975 | 1.594 | -2.665 | -1.475 |
| 6 | 3.585 | 9.146 | 6.234 | 2.415 | -3.146 | -0.234 |
| 5.5 | 4.957 | 6.91 | 5.886 | 0.543 | -1.41 | -0.386 |
| 8 | 8.37 | 11.355 | 8.591 | -0.37 | -3.335 | -0.591 |
| 9.5 | 9.763 | 11.863 | 10.958 | -0.26 | -2.363 | -1.458 |
| 14.5 | 14.883 | 17.378 | 15.198 | -0.383 | -2.878 | -0.698 |
| 17.5 | 17.505 | 18.652 | 17.827 | -0.05 | -1.152 | -0.327 |
| 21 | 21.731 | 22.83 | 21.961 | -0.731 | -1.83 | -0.961 |
| 24 | 23.863 | 24.197 | 23.991 | 0.14 | -0.197 | 0.009 |
| 27 | 25.97 | 27.5 | 27.038 | 1.03 | -0.5 | -0.038 |
| 30.5 | 30.951 | 31.4 | 31.393 | -0.451 | -0.9 | -0.893 |
| 34 | 31.713 | 33.369 | 33.249 | 2.287 | 0.631 | 0.751 |
| 36.5 | 37.101 | 37.789 | 37.663 | -0.601 | -1.289 | -1.164 |
| $\overline{e^2}$ | | | | 1.2637 | 3.4661 | 0.6987 |
| $\overline{e}$ | | | | 0.397 | -1.617 | -0.574 |
| $\sigma^2$ | | | | 1.106 | 0.8514 | 0.3693 |
| Old $\overline{e^2}$ | | | | 0.8667 | 1.5438 | 0.4269 |
| Old $\sigma^2$ | | | | 0.5685 | 0.6771 | 0.3277 |

Table 5.23: Evaluation of the First Set of Data Under D3&D4 Disturbances

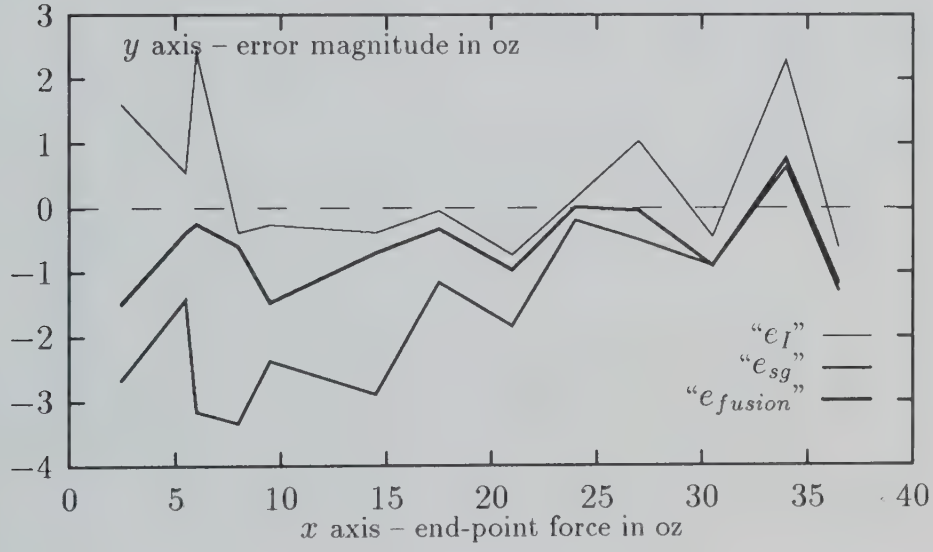


Figure 30: Error Plot When Both Sensors are Under D3&D4

| $F_e$ actual(oz) | $I$ derived(oz) | $V_{out}$ derived(oz) | Fusion (oz) | $e_I$ | $e_{sg}$ | $e_{fusion}$ |
|---|---|---|---|---|---|---|
| 0 | 0.906 | 2.565 | 2.102 | -0.906 | -2.565 | -2.102 |
| 4 | 3.585 | 8.847 | 3.610 | 0.415 | -4.847 | 0.39 |
| 6 | 4.957 | 6.81 | 5.839 | 1.043 | -0.81 | 0.161 |
| 8 | 8.997 | 11.355 | 9.170 | -0.997 | -3.355 | -1.17 |
| 11 | 9.763 | 13.163 | 11.694 | 1.237 | -2.163 | -0.694 |
| 14 | 14.883 | 17.178 | 15.171 | -0.883 | -3.178 | -1.17 |
| 17 | 17.505 | 18.252 | 17.715 | -0.505 | -1.252 | -0.715 |
| 21 | 21.731 | 22.631 | 21.919 | -0.731 | -1.631 | -0.919 |
| 24 | 23.863 | 23.896 | 23.872 | 0.137 | 0.104 | 0.128 |
| 26 | 25.97 | 26.127 | 26.058 | 0.03 | -0.127 | -0.058 |
| 30.5 | 30.961 | 31.501 | 31.496 | -0.46 | -1.01 | -0.996 |
| 33.5 | 31.713 | 33.369 | 33.272 | 1.87 | 0.131 | 0.228 |
| 36.5 | 36.502 | 37.789 | 37.554 | -0.02 | -1.289 | -1.054 |
| $\overline{e^2}$ | | | | 0.7617 | 4.9012 | 0.8707 |
| $\overline{e}$ | | | | 0.0177 | -1.6140 | -0.6131 |
| $\sigma^2$ | | | | 0.7614 | 2.2963 | 0.4948 |
| Old $\overline{e^2}$ | | | | 0.4184 | 1.7702 | 0.3615 |
| Old $\sigma^2$ | | | | 0.3947 | 0.8530 | 0.2760 |

Table 5.24: Evaluation of the Second Set of Data Under D3&D4 Disturbances

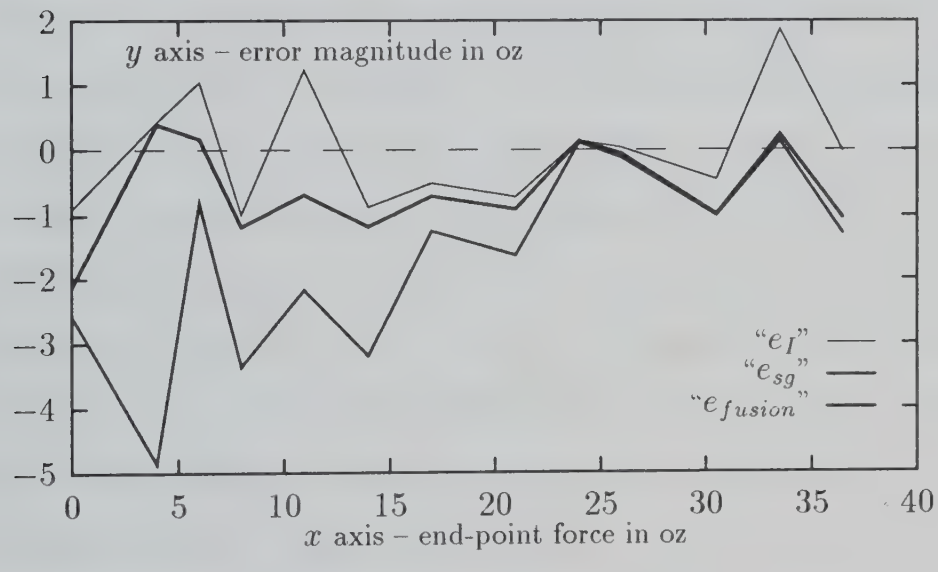


Figure 31: Error Plot When Both Sensors are Under D3&D4

| $\overline{e^2}$ | First Set of Data | | | Second Set of Data | | |
|---|---|---|---|---|---|---|
| | $e_I$ | $e_{sg}$ | $e_{fusion}$ | $e_I$ | $e_{sg}$ | $e_{fusion}$ |
| Case I | 2.2107 | 1.5438 | 0.9692 | 2.2521 | 1.7702 | 0.7289 |
| Case II | 0.8667 | 2.0001 | 0.5630 | 0.4184 | 2.3192 | 0.6262 |
| Case III | 1.2637 | 3.4661 | 0.6987 | 0.7617 | 4.9012 | 0.8707 |
| Old $\overline{e^2}$ | 0.8667 | 1.5438 | 0.4269 | 0.4184 | 1.7702 | 0.3615 |

Table 5.25: Summary of $\overline{e^2}$ for All Cases

| $\sigma^2$ | First Set of Data | | | Second Set of Data | | |
|---|---|---|---|---|---|---|
| | $e_I$ | $e_{sg}$ | $e_{fusion}$ | $e_I$ | $e_{sg}$ | $e_{fusion}$ |
| Case I | 1.7922 | 0.6771 | 0.9600 | 2.1441 | 0.8530 | 0.6349 |
| Case II | 0.5686 | 1.069 | 0.4970 | 0.3947 | 1.2819 | 0.5022 |
| Case III | 1.1060 | 0.8514 | 0.3693 | 0.7614 | 2.2963 | 0.4948 |
| Old $\sigma^2$ | 0.5686 | 0.6771 | 0.3277 | 0.3947 | 0.8530 | 0.2760 |

Table 5.26: Summary of $\sigma^2$ for All Cases

## 5.4 Summary

In this chapter, we studied how the proposed joint torque sensing method performs under Gaussian distributed disturbances. Evaluations were based on the experimental data obtained when no disturbances were considered in the system. Two parameters, mean error square and error variance, are used to compare the fusion results with each independent sensor. In summary, the results in terms of the two parameters are tabulated in Table 5.25 and Table 5.26 respectively for all the cases we studied. From Table 5.26 we conclude that sensor data fusion produces most of the time more convergent errors than that of any single sensor, even though one or more sensors are subject to unmodeled disturbances. In other words, sensor data fusion is generally robust to disturbance due to model uncertainties. In cases where the error variance is slightly bigger than that of a sensor, a more realistic measure of the relative performance is the mean error square shown in Table 5.25, because the sensor seriously diverges from its model and the zero-mean assumption about the

sensor error is no longer valid. In combining with the error variance, the mean error square also serves as a good measure of relative performance, as can be seen from Table 5.25. Therefore, we further conclude that, in order to have the best performance of sensor data fusion, an accurate model of the system is essential and a combination of performance measure is necessary.

# Chapter 6

# Conclusions

## 6.1 Conclusions

We demonstrated the feasibility of the proposed joint torque sensing method via a single-joint robot. The joint torque is obtained by combining motor current sensor and the end-point force sensor. Both sensors are known to contain uncertainties. The statistical *a priori* knowledge of both sensors is obtained from a large number of experiments. The Maximum-Likelihood(ML) fusion algorithm is employed to combine effectively the two sensors based on the statistical knowledge obtained. An evaluation procedure of sensor data fusion is developed and applied to all the experimental data. Robustness of the proposed method to unmodeled disturbances is discussed and demonstrated via experiments. We conclude that the performance of joint torque sensing can be improved by sensor data fusion if the statistical knowledge is available. The improvement under disturbances may be dramatic if an accurate model of the system is provided. Possible extension of works done in our experimental system is

also summarized.

## 6.2 Future Work

We choose to demonstrate the feasibility of the proposed joint torque sensing method in the static case because of reasons summarized in Chapter 4. However, studies of the dynamic case are more challenging due to a number of difficulties. First, the statistical *a priori* knowledge is difficult to obtain accurately because more uncertainties will be involved. One way to overcome this difficulty is to use the knowledge obtained in the static case and then adapt it to the dynamic case according to characteristics of the dynamic system. Secondly, since it is very hard to obtain an accurate model for each part of the system, the performance of the proposed method may degrade if one or more models deviate from its mathematical description. This usually requires adaptive algorithms to compensate the possible degradation of the proposed method. Thirdly, evaluation of sensor data fusion will be more difficult because the end-point force can no longer be compared directly due to the fact that it is hard to measure the end-point force accurately in the dynamic case. Also, the link dynamics may contaminate the derivation of joint torque from the end-point force. Instead of using the end-point force, a set of strain gauges can be mounted directly on the reducer shaft to serve as a comparison basis.

For fusion algorithms in the dynamic case, the Kalman filtering technique is more promising than the ML method we used in the static case. It is known to be effective in dealing with dynamic systems with large amounts of noises. Also, in applying the Kalman technique, we may be able to incorporate the fusion heuristics summarized in section 4.4.3 into the fusion algorithm dynamically by assigning a weight matrix

to the error variance matrix. However, there are also a few foreseeable problems with the Kalman filter technique. The most important one is the determination of the system state equation. Normally, mathematical description of a dynamic system is too complicated to be tractable in real time; therefore, the kinematic model of the system is usually considered for simplicity. Approximations may make one question the creditability of the technique. Further, if the joint torque obtained from fusion algorithm being sent to the input as the torque feedback for real time control, the Kalman filtering technique may cause serious delay problem. Finally, evaluation procedures will not be the same as shown in the static case because of the change of fusion algorithm. In this case, we may choose different criteria for evaluation.

The ultimate goal is to apply this technique to a six DOF robot in general. Before applying this technique, parameter identification and calibration of the real robot are needed. Techniques used in identifying parameters for our single-joint robot are directly applicable. Results obtained in studying the dynamic case should also be applicable directly to a real robot.

Another future work will be the application of the proposed technique. We intend to study the force control algorithms based on the joint torque obtained by our method. Results will be compared to the explicit force control method based on the wrist mounted force/torque sensor only and the motion based force control algorithms. Attention will be focused on the study of stability issues, bandwidth limits and disturbance rejection abilities.

# Bibliography


[1] M. A. Abidi. A regularized multi-dimensional data fusion technique. In *Proc. Inter. Conf. of Robotics and Automation*, pages 2738–2744. IEEE, 1991.

[2] M. A. Abidi and R. C. Gonzalez. The use of multisensor data for robotic applications. *IEEE Transaction on Robotics and Automation*, 6(2):159–177, 1990.

[3] P. Allen and R. Bajcsy. Two sensors are better than one:example of vision and touch. *Third Intern'l Symp. Robotics Research*, pages 48–53, 1985.

[4] Chae H. An, Christopher G. Atkeson, and John M. Hollerbach. Model-based control of a direct drive arm, PartII: Control. In *Proc. Inter. Conf. on Robotics and Automation*, pages 1386–1391. IEEE, 1988.

[5] Chae H. An and John M. Hollerbach. Dynamic stability issues in force control of manipulators. In *Proc. Inter. Conf. of Robotics and Automation*, pages 890–896. IEEE, 1987.

[6] Brian Armstrong. Friction: Experimental determination, modeling and compensation. In *Proc. Inter. Conf. of Robotics and Automation*, pages 1422–1427. IEEE, 1988.

[7] H. Asada, K. Youcef-Toumi, and S. K. Lim. Joint torque measurement of a direct-drive arm. In *Proc. 23rd IEEE Inter. Conf. Decision Contr.*, pages 1332–1337. IEEE, 1984.

[8] Nichola Ayache and Oliver D. Faugeras. Building, registration and fusing noisy visual maps. *The International Journal of Robotics Research*, 7(6):45–65, 1988.

[9] Zixing Cai. *Robotics: Principles and Applications(in Chinese).* South-Central University of Technology Publishing Co., 1987.

[10] Stephen L. Chiu, David J. Morley, and Jim F. Martin. Sensor data fusion on a parallel processor. In *Proc. Inter. Conf. on Robotics and Automation*, pages 1629–1633. IEEE, 1986.

[11] James J. Clark and Alan L. Yuille. *Data Fusion for Sensory Information Processing Systems.* Kluwer Academic Publisher, 1990.

[12] Paolo Dario(editor). *Sensors and Sensory Systems for Advanced Robots.* Springer-Verlag Berlin Heidelberg, 1988.

[13] C. Canudas de Wit and K. J. Astrom. Adaptive friction compensation in dc-motor drives. *IEEE Journal of Robotics and Automation*, RA-3(6):681–685, 1987.

[14] C. Canudas de Wit and A. Aubin. Robot parameter identification via sequential hybrid estimation algorithm. In *Proc. Inter. Conf. on Robotics and Automation*, pages 952–1957. IEEE, 1991.

[15] C. Canudas de Wit et al. Adaptive friction compensation in robot manipulators:loow velocities. *The International Journal of Robotics Research*, 10(3):189–199, 1991.

[16] Hugh F. Durrant-Whyte. Consistent integration and propagation of disparate sensor observations. *The International Journal of Robotics Research*, 6(3):3–24, 1987.

[17] P. Elosegui, R. W Daniel, and P. M Sharkey. Joint servoing for robust manipulator force control. In *Proc. Inter. Conf. on Robotics and Automation*, pages 246–251, 1990.

[18] Steven D. Enpinger and Warren P. Seering. On dynamic models of robot force control. In *Proc. Inter. Conf. of Robotics and Automation*, pages 29–34. IEEE, 1986.

[19] Steven D. Enpinger and Warren P. Seering. Understanding bandwidth limitations in robot force control. In *Proc. Inter. Conf. of Robotics and Automation*, pages 904–909. IEEE, 1987.

[20] Harmon C. Fowler and Steven D. Eppinger. Bandwidth performance of a direct drive manipulator under joint torque and endpoint force control. In *Proc. Inter. Conf. of Robotics and Automation*, pages 230–237. IEEE, 1991.

[21] Gene F. Franklin, J. David Powell, and Michael L. Worman. *Digital Control of Dynamic Systems.* Addison-Wesley Publishing Company, 1990.

[22] J. K. Hackett and Mubarak Shah. Multi-sensor fusion. Technical report, Univ. of Central Florida, Orlando, FL 32816., CS-TR-89-16.

[23] S. Y. Harmon, G. L. Bianchini, and B. E. Pinz. Sensor data fusion through a distributed blackboard. In *Proc. Inter. Conf. on Robotics and Automation*, pages 1449–1454. IEEE, 1986.

[24] M. Hashimoto and R. P. Paul. Integration of manipulator joint sensor information for robust robot control. In *Proc. 26th Conf. on Decision and Control*, pages 603–604, 1987.

[25] Minoru Hashimoto. Robot motion control based on joint torque sensing. In *Proc. Inter. Conf. on Robotics and Automation*, pages 256–261. IEEE, 1989.

[26] Minoru Hashimoto et al. A joint torque sensing technique for robots with Harmonic drives. In *Proc. Inter. Conf. on Robotics and Automation*, pages 1034–1039. IEEE, 1991.

[27] Minoru Hashimoto and Toshiro Horiuchi. The effects of joint flexibility on robot motion control based on joint torque positive feedback. In *Proc. Inter. Conf. of Robotics and Automation*, pages 1220–1225. IEEE, 1991.

[28] Minoru Hashimoto and R. P. Paul. Integration of multi-sensor manipulator actuator information for robust robot control systems. Technical report, Kagoshima University, Kagoshima 890, Japan, 1989.

[29] Neville Hogan. Impedance control: An approach to manipulation: Part I. *Journal of Dynamic Systems, Measurement, and Control*, 107:1–7, 1985.

[30] O. Khatib. A unified approach for motion and force control of robot manipulator:the operational space formulation. *IEEE Journal of Robotics and Automation*, RA-3(1):43–53, 1987.

[31] V. D. Kostadinov. Geometric parameters estimation of robotic systems. In *Proc. Inter. Conf. on Robotics and Automation*, pages 964–969. IEEE, 1991.

[32] Kazuhiro Kosuge, H. Takeuchi, and Katsuhisa Furuta. Motion control of a robot arm using joint torque sensors. *IEEE Transaction on Robotics and Automation*, 6(2):258–263, 1990.

[33] J.Y.S. Luh, William D. Fisher, and Richard P. Paul. Joint torque control by a direct feedback for industrial robots. *IEEE Transaction on Automatic Control*, AC-28(2):153–161, 1983.

[34] Ren C. Luo, Min-Hsiung Lin, and Ralph S. Scherp. Dynamic multi-sensor data fusion system for intelligent robots. *IEEE Journal of Robotics and Automation*, 4(4):386–396, 1988.

[35] Nirode Mohanty. *Signal Processing.* Van Nostrand Reinhold Company, 1987.

[36] Wyatt S. Newman and Jay J. Patel. Experiments in torque control of the AdeptOne robot. In *Proc. Inter. Conf. of Robotics and Automation*, pages 1867–1872. IEEE, 1991.

[37] OMEGA Inc. *The Pressure Strain And Force handbook*, 1990/91. Vol. 27.

[38] Lawrence E. Pfeffer, Oussama Khatib, and John Hake. Joint torque sensory feedback in the control of a PUMA manipulator. *IEEE Transaction on Robotics and Automation*, 5(4):418–425, 1989.

[39] E. P. Popov. *Mechanics of Materials.* Prentice-Hall, 1976.

[40] M. H. Raibert and J. J. Craig. Hybrid position/motion control of manipulators. *ASME Journal of Dynamic Systems, Measurement, and Control*, 103(2):126–133, 1981.

[41] B. Raucent and G. Campion. On the identification of the barycentric parameters of robot manipulators from external measurements. In *Proc. Inter. Conf. on Robotics and Automation*, pages 1169–1174. IEEE, 1991.

[42] John M. Richardson and Kenneth A. Marsh. Fusion of multisensor data. *The International Journal of Robotics Research*, 7(6):78–96, 1988.

[43] Corinne C. Ruokangas, Michael S. Black, Jim F. Martin, and Jeffrey S. Schoenwald. Integration of multiple sensors to provide flexible control strategies. In *Proc. Inter. Conf. on Robotics and Automation*, pages 1947–1953. IEEE, 1986.

[44] J. K. Salisbury. Active stiffness control of a robot manipulator in cartesian control. In *Proc. IEEE Conf. Decision and Control*, pages 95–100. IEEE, 1980.

[45] G. Seeger and W. Leonhard. Estimation of rigid body models for a six-axis manipulator with geared electric drives. In *Proc. Inter. Conf. on Robotics and Automation*, pages 1690–1695. IEEE, 1989.

[46] Kang G. Shin and Chih-Ping Lee. Compliance control of robotic manipulation with resolved acceleration. In *Proc. Inter. Conf. on Robotics and Automation*, pages 350–357. IEEE, 1985.

[47] William T. Townsend and Jr. J. Kennethe Salisbury. The effect of Coulomb friction and stiction on force control. In *Proc. Inter. Conf. of Robotics and Automation*, pages 883–889. IEEE, 1987.

[48] Michael W. Walker, Al Dobryden, and Joseph Dionise. Getting to know your robot. In *Proc. Inter. Conf. on Robotics and Automation*, pages 1245–1250. IEEE, 1990.

[49] Chi-haur Wu and Richard P. Paul. Manipulator compliance based on joint torque control. In *Proc. 19th IEEE Inter. Conf. Decision Contr.*, pages 88–94. IEEE, 1980.

[50] Yuan F. Zheng. Integration of multiple sensors into a robotic system and its performance evaluation. *IEEE Transaction on Robotics and Automation*, 5(5):658–669, 1989.

B45972